Materials Advances

PAPER

Check for updates

A TiO₂ grafted bamboo derivative nanocellulose polyvinylidene fluoride (PVDF) nanocomposite membrane for wastewater treatment by a photocatalytic process

Md Rezaur Rahman, [ID] *[a] Anthonette James,[a] Khairul Anwar Mohamed Said,[a] Murtala Namakka, [ID][a] Mayeen Uddin Khandaker,[b] Woo Haw Jiunn, [ID][c] Jehan Y. Al-Humaidi, [ID][d] Raed H. Althomali [ID][e] and Mohammed Muzibur Rahman [ID][f]

The escalating demands for efficient wastewater treatment drive this study, which explores the development and characterization of polyvinylidene fluoride (PVDF) nanocomposite membranes enhanced with nanocellulose (NC) and titanium dioxide (TiO₂). The integration of NC and TiO₂ nanoparticles into a PVDF matrix *via* the phase inversion method yielded notable improvements in the structural, mechanical, and functional properties of the membranes. Fourier-transform infrared spectroscopy (FTIR) analysis confirmed the presence of critical functional groups that facilitated improved interactions within the nanocomposite membrane. These interactions contributed to the enhanced membrane hydrophilicity, suggesting their potential to improve water permeability. Field emission scanning electron microscopy (FESEM) revealed the uniform dispersion of TiO₂ and NC at optimal loadings, which minimized nanoparticle agglomeration and promoted the formation of a more porous and permeable membrane structure. X-ray diffraction (XRD) showed an increase in the crystallinity of the β-phase of PVDF, thus enhancing mechanical stability and overall membrane functionality. The optimization of TiO₂ loading at 3 wt% resulted in maximum efficacy, with a 15% increment in water flux rates from 234.06 L m⁻² h⁻¹ to 270.23 L m⁻² h⁻¹ over an unmodified PVDF/NC membrane and achieving methylene blue (MB) dye rejection rates of up to 98%. The enhanced physical properties of the membrane, resulting from a reduction in mean pore size from 0.00488 to 0.00470 μm and improved porosity from 76.07% to 79.68% ensured more effective filtration. These modifications have surpassed the performance of the unmodified PVDF/NC membrane. Additionally, the presence of TiO₂ nanoparticles significantly enhanced the photocatalytic properties of the membranes, accelerating the degradation of MB pollutants and improving antifouling properties. This was evidenced by the high flux recovery rate (FRR) percentage, which underscores their superior self-cleaning capabilities. These findings illustrate that the synergistic integration of NC and TiO₂ not only capitalized on the individual properties of each component but also significantly elevated overall membrane performance and maintained longevity in their practical usage. This study represents a significant advancement in membrane technology, offering new avenues for sustainable and efficient environmental remediation and presenting robust solutions to challenges such as membrane fouling.

ᵃ Department of Chemical Engineering and Energy Sustainability, Faculty of Engineering, University Malaysia Sarawak, Kota Samarahan, 94300, Malaysia.
E-mail: rmrezaur@unimas.my
ᵇ Applied Physics and Radiation Technologies Group, CCDCU, School of Engineering and Technology, Sunway University, 47500, Bandar Sunway, Selangor, Malaysia
ᶜ Centre for Ionics University of Malaya, Department of Physics, Faculty of Science, University of Malaya, 50603 Kuala Lumpur, Malaysia
ᵈ Department of Chemistry, College of Science, Princess Nourah bint Abdulrahman University, P.O. BOX 84428, Riyadh 11671, Saudi Arabia
ᵉ Department of Chemistry, College of Art and Science, Prince Sattam bin Abdulaziz University, Wadi Al-Dawasir 11991, Al Kharj, Saudi Arabia
ᶠ Center of Excellence for Advanced Materials Research (CEAMR) & Department of Chemistry, Faculty of Science, King Abdulaziz University, Jeddah 21589, Saudi Arabia

1. Introduction

Access to safe and clean water is not only a fundamental human right but also a cornerstone of global health and sustainable development.[1] Despite international commitments and advancements in technology, over 2.1 billion people worldwide still lack reliable access to clean water, plunging communities into cycles of poverty and illness.[2] The World Health Organization estimates that around 3.4 million lives are lost annually due to water-related diseases, underscoring the urgency of addressing water scarcity and pollution. The situation is exacerbated by rapid industrialization, which significantly contributes to water contamination through the discharge of organic dyes and oily wastewaters from sectors such as textiles, metallurgy, and pharmaceuticals.[3] Industrial effluents, particularly those containing hazardous dyes and heavy metals, pose profound challenges to environmental and public health.[4] Dyes, used extensively in various industries, are notorious for their visibility and resistance to degradation, leading to significant ecological disruptions when discharged untreated into aquatic ecosystems.[5]

The persistence of these contaminants in water bodies is a testament to the inefficiencies of traditional water treatment methods, which often struggle with high operational costs, secondary pollution, and limited effectiveness in removing complex pollutants.[6] One of the primary limitations of conventional polymeric membranes in water treatment systems is their susceptibility to fouling, which negatively impacts membrane performance over time.[7] Fouling occurs when particulates start to accumulate or adsorb onto the membrane surface, leading to both internal and external clogging and reduced permeability. This problem significantly increases the operation costs of treatment systems due to the need for membrane cleaning and replacement.[8] However, a study has shown that integrating a new material[9] such as MXene into a membrane system can prolong its lifespan due to its antifouling properties[10] This aids in conserving membrane efficiency and minimizing the frequency of cleaning and replacement. Despite these advancements, the study lacks a comprehensive evaluation of the potential toxicity of MXene to the ecosystem.

To combat these challenges, there has been a marked shift towards innovative technologies that promise not only efficacy but also sustainability and eco-friendliness in water treatment processes. One such innovative approach is the inclusion of nanocellulose derived from natural fibers, which offers a distinctive edge in wastewater treatment due to its intrinsic hydrophilic nature, excellent biocompatibility, and modifiable surface chemistry.[11–13] These inherent properties make nanocellulose a promising candidate for improving the development of membranes, while the shift toward sustainable practices improves the value of renewable and biodegradable materials. However, previous studies have observed that the properties of nanocellulose membranes still fall short of fulfilling the demands for high strength and durability requirements needed for extended operation usage.[13–15] In this regard, photocatalytic technology and membrane separation have emerged as pivotal

solutions to further enhancing the performance of membranes.[16] With its high specific surface area and exceptional physicochemical properties, nanocellulose synergizes effectively with other nanomaterials, leading to enhanced hybrid membrane properties that closely mimic those of commercial membranes.[12,17] As such, the incorporation of inorganic nanomaterials such as titanium dioxide (TiO_2),[9] graphene oxide (GO), zinc sulfide (ZnS), magnesium oxide (MgO), iron(III) oxide (Fe_2O_3), and carbon nanotubes (CNTs) as fillers within membranes has opened up new opportunities for enhancing membrane performance.[18–20] The literature shows that the presence of nanoparticles in the membrane enhances its strength, hydrophilicity, porosity, and charge density, which in turn increases efficiency, permeability, and fouling resistance.[21,22] Considering this, the incorporation of TiO_2 nanoparticles into nanocellulose membranes addresses the shortcomings of current membrane technologies with the addition of photocatalytic and antifouling properties, thereby imparting self-cleaning capabilities to the membrane.

Integrating photocatalysts with membrane technologies, which feature low energy consumption and minimal secondary pollution, can enhance the sustainability and efficiency of water treatment systems.[23] The paradigm of process intensification (PI) presents a transformative approach to industrial processes, including water treatment.[24] PI aims to minimize the environmental footprint of manufacturing while maximizing process efficiency, aligning with sustainable development goals.[25] By adhering to principles such as maximizing the effectiveness of molecular interactions and optimizing process scales, PI encourages the adoption of advanced manufacturing technologies like continuous processing and hybrid separation techniques.[26] Such innovations are crucial for reducing energy consumption, raw material costs, and waste generation, offering a more robust framework for environmental stewardship and economic viability.

Membrane technology, in particular, has gained significant traction as a tool for PI in water treatment.[27] The integration of membrane-based separations into intensified processes facilitates more effective removal of pollutants while reducing operational costs and energy usage.[28] This technology not only supports the sustainable management of water resources but also enables the recovery of valuable by-products from wastewater, thus contributing to a circular economy.[29] In light of these advancements, there is a compelling need for continued research and development in membrane and photocatalytic technologies.[30] The synergy between these technologies can potentially revolutionize wastewater treatment facilities, making them more efficient and less reliant on conventional, resource-intensive methods.[31] As the world moves towards a future where water scarcity and pollution are likely to present even greater challenges, the role of engineering in innovating and implementing effective, sustainable solutions becomes increasingly critical.[32] This study aims to explore the latest developments in process intensification and membrane technology by investigating the enhancement of polyvinylidene fluoride/nanocellulose (PVDF/NC) nanocomposite membranes

through the incorporation of varying loading percentages of TiO$_2$ nanoparticles. By observing their influence on membrane performance, particularly in terms of photodegradation effectiveness, the study emphasizes the synergistic compatibility of NC and TiO$_2$ in mitigating the global water crisis and paving the way for a water-secure world, especially in Sarawak. The presence of advanced technologies supports the ongoing efforts to develop robust and sustainable approaches for addressing water scarcity issues in order to ensure a cleaner and more sustainable future for our region.

2. Methodology

2.1 Materials

In the preparation of PVDF/NC and PVDF/NC/TiO$_2$ nanocomposite membranes, nanocellulose (NC) derived from bamboo was extracted from *Gigantochloa scortechinii* species. Chemicals such as poly(vinylidene fluoride) (PVDF) (CAS no. 24937-79-9, molecular weight: 534 000 g mol^{-1}), lithium chloride (LiCl) (CAS no. 7447-41-8), titanium(IV) oxide (CAS no. 13463-67-7), and dimethylacetamide (DMAc) (CAS no. 127-19-5) were supplied by Sigma Aldrich Sdn (Petaling Jaya, Malaysia). Both ultrapure water and deionized (DI) water used in the experiment work were provided by Universiti Malaysia Sarawak (UNIMAS). All of the listed chemicals were of analytical grade.

2.2 Preparation of PVDF/NC and PVDF/NC/TiO$_2$ nanocomposite membranes

The nanocomposite membranes were prepared *via* the phase inversion technique followed by the non-solvent-induced phase separation (NIPS) method.[33,34] Initially, NC and LiCl, a pore-forming additive were dissolved in DMAc solvent at a temperature of 165 °C until a homogeneous solution was obtained to improve the porous structure of the developed membrane. Following this, the temperature of the dope solution was reduced to 50 °C and TiO$_2$ was added within the range of 2–4% based on the literature findings highlighting its superior antifouling properties and self-cleaning ability.[33,35] Finally, PVDF pellets were gradually added into the homogeneous dope solution and subjected to continuous stirring at a constant temperature of 50 °C and 350 rpm for 24 hours to achieve homogeneity and reduce air bubbles. The material composition of each developed membrane was prepared according to the loadings tabulated in Table 1. After the completion of the 24-hour dissolution process, approximately 10 mL of the dope solution was poured onto a glass plate (21 cm × 30 cm) for

the membrane casting process at room temperature. The cast membrane was initially immersed in the first coagulation bath containing DI water for 20 minutes to facilitate the elimination of solvent and non-solvent additives *via* a phase separation process and to initiate membrane solidification. Subsequently, the membrane was transferred to the second coagulation bath containing DI water and left for 24 hours to remove any excess solvent retained within the membrane matrix, which could potentially affect its properties. Finally, the membrane was kept in a container and soaked in ultrapure water before being stored in the refrigerator (5 °C) until further characterization.

2.3 Nanocomposite membrane characterization

2.3.1 Fourier transform infrared spectroscopy (FTIR). FTIR 'IRAffinity-1' spectroscopy (Shimadzu; Japan) was used to identify the functional groups and the structures of molecular bonds through the observation of IR spectrum bands at a range of 4000 to 400 cm^{-1}. For ATR-FTIR, the solid membrane sample (1 cm × 1 cm) was cut and placed onto the holder known as the ATR-FTIR crystal. The swivel press was used to press down the sample and crystal, ensuring the sample-crystal was in contact. Analysis of qualitative and quantitative aspects of the FTIR spectrum was based on the standards of ASTM E1252-98 (2021) as well as ASTM E168-16 (2016).[36,37]

2.3.2 Field emission scanning microscopy (FE-SEM) and energy dispersive X-ray (EDX). A Hitachi S-4700 FESEM was used to observe the morphological images of the membrane samples. The sample was mounted on aluminium stubs and later fine-coated using 'JFC-1600' (JEOL (Japan) Ltd). Images of the sample surface were captured using a field emission gun with a voltage of 20 kV. This procedure was performed based on the standard of ASTM E3-11 (2017).[38]

While FESEM provides information about the morphological characteristics of the sample, EDX was employed to analyze the sample elemental compositions.

2.3.3 X-ray diffraction analysis (XRD). XRD analysis was performed to determine the crystallinity of the samples and to observe the presence of crystalline phases. The membrane samples were analyzed at room temperature using a Rigaku SmartLab Powder X-ray diffractometer with CuKα radiation (λ = 1.5418 Å). The XRD patterns of all samples were recorded within a scattering angle (2θ) ranging from 5 to 90° at a scanning rate of 2 min^{-1}. The crystalline index (CrI) was identified using an empirical eqn (1), whereas the crystallite size was calculated using Debye Scherrer eqn (2). This procedure

Table 1 Dope solution compositions

Membrane sample	PVDF (wt%)	DMAc (wt%)	LiCl (wt%)	TiO$_2$ (wt%)	NC (wt%)
S0-PVDF/NC	15	84.06	0.34	0	0.6
S1-PVDF/NC/TiO$_2$	15	83.76	0.34	0.3	0.6
S2-PVDF/NC/TiO$_2$	15	83.69	0.34	0.375	0.6
S3-PVDF/NC/TiO$_2$	15	83.61	0.34	0.45	0.6
S4-PVDF/NC/TiO$_2$	15	83.54	0.34	0.525	0.6
S5-PVDF/NC/TiO$_2$	15	83.46	0.34	0.6	0.6

was carried out in accordance with the ASTM F3419-22 (2022) standard.[39]

$$\text{Crystalline index } (\%) = \frac{\text{area of all the crystalline peak}}{\text{area of the crystalline} + \text{amorphous peaks}} \times 100 \tag{1}$$

$$D = \frac{k\lambda}{\beta \cos\theta} \tag{2}$$

where, k: 0.94 (Scherrer constant); $\lambda = 1.5418$ nm (X-ray wavelength); β: line broadening at full width at half maximum (FWHM) in radians.

2.3.4 Membrane porosity and mean pore measurement. The membrane porosity (ε) was determined using the gravimetric method based on eqn (3).[40]

$$\varepsilon\% = \frac{\left(\frac{W_{\text{wm}} - W_{\text{dm}}}{\rho_{\text{water}}}\right)}{\left(\frac{W_{\text{wm}} - W_{\text{dm}}}{\rho_{\text{water}}}\right) + \left(\frac{W_{\text{dm}}}{\rho_{\text{PVDF}}}\right)} \times 100 \tag{3}$$

where, w_{wm}: weight of wet membrane (g), w_{dm}: weight of dry membrane (g), ρ_{water}: density of water (0.998 g cm^{-3}) and ρ_{PVDF}: density of PVDF polymer (1.740 g cm^{-3}).

Meanwhile, the mean pore size of the membrane was calculated following the Guerout–Elford–Ferry equation.[41] The mean pore radius was obtained from eqn (4) and the mean pore diameter was determined by multiplying the value of the mean pore radius by two (eqn (5)).

$$\text{Mean pore radius} = \sqrt{\frac{(2.9 - 1.75\varepsilon) \times 8\eta l Q}{\varepsilon \times A \times \Delta P}} \tag{4}$$

where, ε: membrane porosity (%), η: water viscosity (0.00089 Pa s), l: membrane thickness, Q: volume of water permeation (m^3 s^{-1}), A: effective area of membrane and Δ: pressure applied (Pa).

$$\text{Mean pore size (nm)} = 2 \times \text{mean pore radius} \tag{5}$$

2.3.5 Ultraviolet-visible (UV-vis) spectroscopy for dye removal concentration analysis. Approximately 5 mL of the sample was pipetted onto the UV-vis cuvette and then placed into the UV-vis spectrophotometer for analysis. The wavelength was set between 500 to 700 nm for MB dye solution. A calibration curve was developed using reference compounds of known concentration (0.1, 0.2, 0.5, 1.0 ppm of MB). The test was performed in accordance with the ASTM E169-16 (2022).[42]

2.4 PVDF/NC and PVDF/NC/TiO$_2$ nanocomposite membrane performance evaluation

The study was conducted in three successive procedures to evaluate their water permeability and methylene blue (MB) dye selectivity with experimental conditions detailed in each subsection.

2.4.1 Nanocomposite membrane water permeation flux analysis. Each flat sheet nanocomposite membrane sample measuring 4.4 cm in diameter was cut and placed onto the
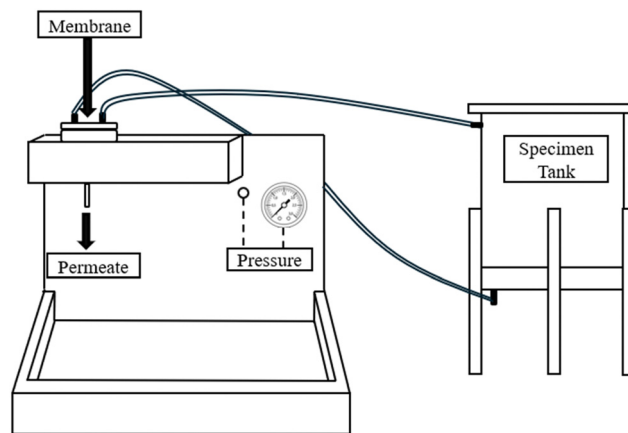

Fig. 1 Schematic diagram of the water filtration system.

membrane holder of the water filtration machine, as displayed in Fig. 1. The membrane was secured by tightening a rubber O-ring around it, which held the membrane in place and locked the membrane into position using the membrane holder cover. This machine featured an effective membrane filtration area of 1.52×10^{-3} m^2. Initially, the membrane was pre-compressed for 30 minutes at 2 bar pressure to allow for a stable flux before the actual measurements commenced. Afterward, the pressure was reduced to 1 bar and the volume of the permeate was recorded every 10 minutes for a 70-minute analysis. The applied pressure in the system served as the driving force for water permeation through the membrane. The water permeation flux resulting from the application of the subjected membrane was calculated by determining the ratio of permeate volume to permeation time, following eqn (6).[41] Each membrane sample was subjected to five water permeation flux tests in order to determine their average and standard deviation.

$$J_{\text{W}} = \frac{V}{A \times \Delta T} \tag{6}$$

where, J_{W}: pure water permeation flux (L m^{-2} h^{-1}), V: permeate volume (m^3), A: effective area of membrane (m^2) and ΔT: filtration time (h).

2.4.2 Nanocomposite membrane dye removal analysis. MB dye with a concentration of 1 ppm was used in the study as the feed for the membrane removal test analysis. The initial dye concentration was confirmed using a UV-160 UV-Vis-NIR spectrophotometer (Shimadzu Scientific Instruments, Inc., Tokyo, Japan). Upon starting the experiment, 1000 mL of 1 ppm MB dye solution was poured into the solution tank and the pressure applied on the membrane was set to 1 bar at room temperature. The permeate (J_{MB}) was collected and its volume was recorded at 10-minute intervals for a 70-minute analysis. The dye removal ratio (R) was determined using eqn (7).[43] Each membrane sample was subjected to five dye removal tests in order to determine their average and standard deviation.

$$\% R = \left(1 - \frac{C_{\text{f}}}{C_{\text{i}}}\right) \times 100 \tag{7}$$

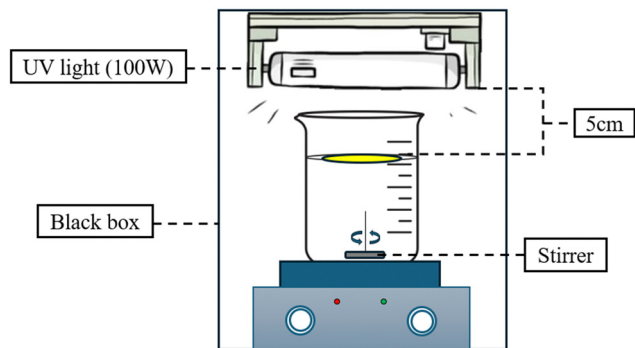**Fig. 2** Experimental setup for photocatalytic activity.

where, R: dye removal ratio (%), C_f: final MB dye concentration (mg L^{-1}), C_i: initial MB dye concentration (mg L^{-1}).

2.4.3 Nanocomposite membrane antifouling performance. After the MB dye removal test, each nanocomposite membrane was subjected to photocatalytic activity in the presence of UV light irradiation, as illustrated in Fig. 2. This procedure was carried out to evaluate the self-cleaning performance of the nanocomposite membrane. Initially, the used nanocomposite membrane after the dye removal test was submerged in a Petri dish containing 50 mL of DI water which was then exposed to a 100 W UV light irradiation, positioned 5 cm just above the membrane surface for 24 hours in a dark space. The cleaned nanocomposite membrane was subsequently subjected to another water permeation flux (J_{W2}) test for a second time with constant operating conditions as previously mentioned. The flux recovery ratio (FRR) of the nanocomposite membrane was calculated using eqn (8).[43] The dye removal test was repeated 5 times for each membrane to ensure the accuracy of the result.

$$\text{FRR} = \left(\frac{J_{w2}}{J_w} \right) \times 100\% \tag{8}$$

where, J_W: initial pure water permeation flux (L m^{-2} h^{-1}), J_{W2}: pure water permeation flux after photocatalytic activity.

3. Results and discussion

3.1 The FTIR analysis of the nanocomposite membranes

The FTIR spectra of the main materials used to fabricate nanocomposite membranes are shown in Fig. 3(a) and (b), while Fig. 4 shows the functional groups present in PVDF/NC and PVDF/NC/TiO$_2$ nanocomposite membranes. Based on the analysis in Fig. 3(a), the peaks detected at a wavenumber of 875.68 cm^{-1} and 1174.65 cm^{-1} revealed the stretching vibration of C–C and CF$_2$ of PVDF.[44] Meanwhile, the appearance of the peak at 1396.46 cm^{-1} signified the bending vibration of CH$_2$ in the PVDF polymer.[41] The aforementioned peaks became more pronounced in Fig. 4 when incorporating both nanocellulose and TiO$_2$ into the PVDF matrix, which resulted in enhanced interaction and consequently led to improved structural integrity. In Fig. 4, all nanocomposite membranes labeled S1–S5 exhibited distinct bands at 839 cm^{-1} and showed a slightly deviated peak at 879 cm^{-1} compared to the previous peak that appeared at 875.68 cm^{-1} in Fig. 3(a). These peaks corresponded to the robust vibrational bands characterizing the β phase of PVDF, which correlated with the XRD results shown in Fig. 6. According to the literature, the solvent-casting approach of PVDF nanocomposite membranes prepared using a dipolar aprotic solvent such as DMac has resulted in the formation of a predominant β-phase membrane structure.[41,43] One of the influencing factors was the retention of residual solvent within the PVDF nanocomposite matrix, which significantly affected the membrane crystalline structure.[45,46] The impact was evident in a study using hexamethyl phosphoramide (HMPA), where the initial stage of the membrane drying process left a significant solvent residual of 71%, resulting in the formation of a β-phase membrane.[45] However, the
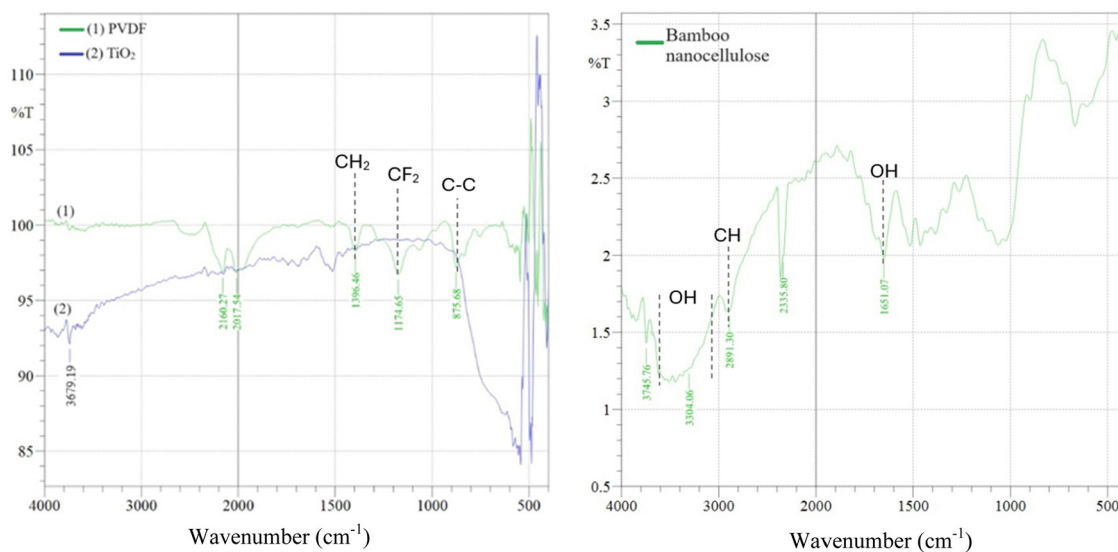

Fig. 3 FTIR spectra of (a) PVDF pellet and TiO$_2$ nanoparticles and (b) bamboo nanocellulose.
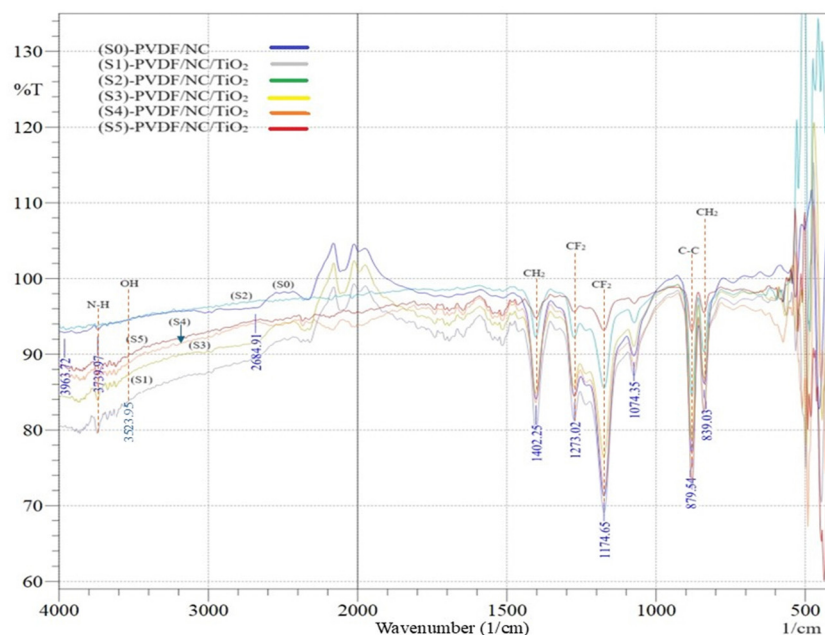
Paper

Fig. 4 Comparison between the FTIR spectra of PVDF/NC and PVDF/NC/TiO$_2$ nanocomposite membranes with varying TiO$_2$ loading.

crystalline structure of the membrane gradually changed as the percentage of residual solvent was reduced.

In Fig. 3(a) and (b), an absorption peak within the spectral range of 3700–2995 cm^{-1} signified the presence of hydroxyl (OH) stretching vibrations of alcohol or phenol within the TiO$_2$ nanoparticles and bamboo nanocellulose. In the TiO$_2$ nanoparticles, the detected OH stretching vibration peak was identified as a free radical OH species without hydrogen bonding.[47] The existence of these free hydroxyl radicals played an important role in initiating the photocatalytic activity of TiO$_2$ nanoparticles within the developed nanocomposite membrane. Their presence facilitated the breakdown of organic pollutants in wastewater when subjected to light sources during the membrane treatment process.[48] Meanwhile, the detection of OH stretching vibration in bamboo nanocellulose samples was common due to the presence of hydroxyl groups attached to the carbon backbone in the glucose units.[11,49] The band observed at 2891 cm^{-1} was assigned to the symmetrical stretching vibration of the C–H bond in the fiber samples.[50] This peak was found to represent the general organic components in polysaccharide samples.[51] Fig. 3(b) detects another hydroxyl functional group at 1651 cm^{-1}. This peak corresponded to the hygroscopic nature of nanocellulose, which contributes to the hydrophilicity characteristics of the developed PVDF/NC/TiO$_2$ nanocomposite membrane, thereby enhancing water permeability through the membrane.[52–54]

The FTIR spectra depicted in Fig. 4 provided a comparative analysis between PVDF/NC and PVDF/NC/TiO$_2$ nanocomposite membranes. Similar trends were observed across all nanocomposite samples labeled S0–S5. The incorporation of NC and TiO$_2$ into the PVDF matrix induced an O–H stretching vibration at 3525 cm^{-1} in the nanocomposite membrane samples. This distinctive peak signaled the presence of hydrophilic additives within the fabricated membrane structure. Apart from that, peaks within the range of 839 cm^{-1} to 1402 cm^{-1} became more pronounced compared to the peak shown by the PVDF pellet in Fig. 3(a). These peaks corresponded to the functional groups associated with the stretching vibration of C–C, CF$_2$ and CH$_2$ which were influenced by the dipolar interaction between the PVDF polymer and the organic solvent DMac during the dope solution preparation.[55] A similar absorption band at 3745.70 cm^{-1} was observed in both PVDF/NC and PVDF/NC/TiO$_2$ nanocomposite membranes. This band was attributed to the treatment approach of bamboo nanocellulose.[11,56] This treatment introduced new functional groups of N–H on the surface of nanocellulose, which play a significant role in improving the compatibility barrier between nanocellulose and the PVDF matrix. Hence, the combination of the hydrophilic characteristics of nanocellulose and its improved surface chemistry holds excellent potential in minimizing the fouling issues encountered in a membrane system.[57]

3.2 The FESEM and EDX analysis of the nanocomposite membranes

The surface and cross-sectional morphologies of the PVDF/NC and PVDF/NC/TiO$_2$ nanocomposite membranes featuring varying percentages of TiO$_2$ nanoparticles are presented in Fig. 5 and 6 using field emission scanning electron microscopy (FESEM) analysis, respectively. Based on the analysis, all membrane surface morphologies showed interconnected patterns where both open pores and cracks were visible. The surface morphologies presented in Fig. 5 exhibited several cracks dispersed across the surface that possibly resulted from unintended stress during the membrane fabrication. The presence of pores was further confirmed by the cross-sectional images shown in Fig. 6, which highlighted the
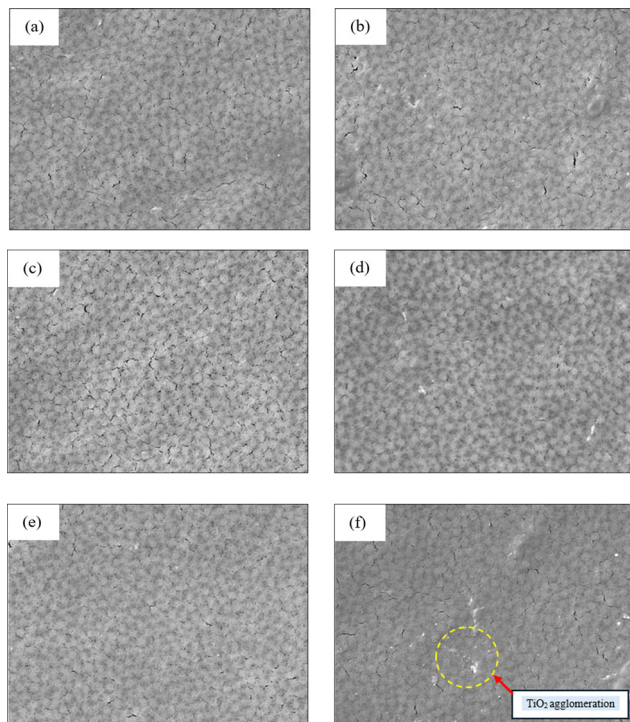
Fig. 5 FESEM images of membrane surface configurations at 10 000× magnification: (a) S0-PVDF/NC, (b) S1-PVDF/NC/TiO₂, (c) S2-PVDF/NC/TiO₂, (d) S3-PVDF/NC/TiO₂, (e) S4-PVDF/NC/TiO₂, (f) S5-PVDF/NC/TiO₂.
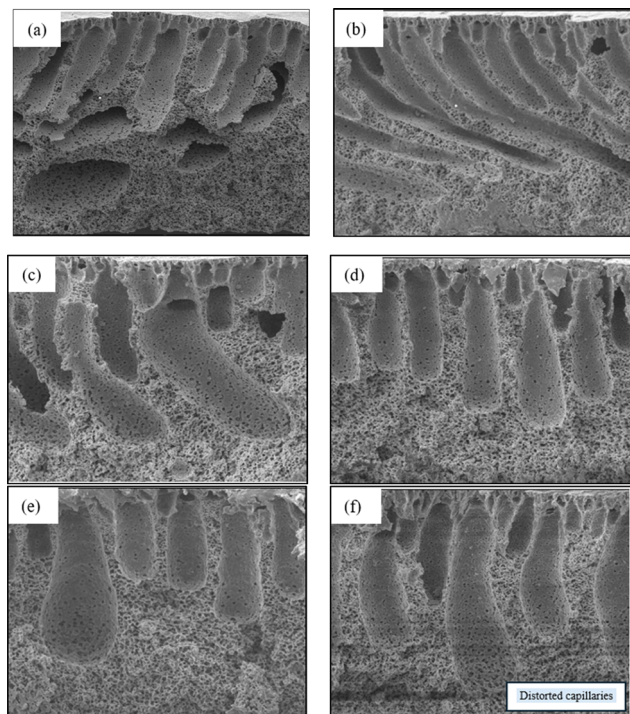
Fig. 6 FESEM images of membrane cross-sectional configurations at 1500× magnification: (a) S0-PVDF/NC, (b) S1-PVDF/NC/TiO₂, (c) S2-PVDF/NC/TiO₂, (d) S3-PVDF/NC/TiO₂, (e) S4-PVDF/NC/TiO₂, (f) S5-PVDF/NC/TiO₂.

formation of the pores at the bottom surface of all membranes. The formation of open pores at the top layer of the membrane was accelerated by the inclusion of lithium chloride (LiCl), which served as the pore-forming additive altering the solvent-non-solvent exchange rate during the membrane phase inversion process.[58,59] Fig. 5(a) displays the pristine S0-PVDF/NC membrane without TiO₂ loading. A notable distinction was observed in the surface morphology of the nanocomposite membrane S5-PVDF/NC/TiO₂ in Fig. 5(f), which had the highest percentage of TiO₂ nanoparticle loading. In particular, some spots covered with a layer of TiO₂ over the substrate were evident in the image representing S5-PVDF/NC/TiO₂. This observation was attributed to the non-uniform dispersion of the TiO₂ nanoparticles as the percentage of TiO₂ loadings increased, thereby causing agglomeration issues. The presence of the TiO₂ nanoparticles on the surface morphology of the respective nanocomposite membrane was confirmed by the energy dispersive X-ray spectroscopy (EDX) analysis which is shown in Table 2. In contrast, the other PVDF/NC/TiO₂ nanocomposite membranes shown in Fig. 5(b)–(e) exhibited a less prominent appearance of TiO₂ loadings on their membrane surfaces due to the filling density of TiO₂ in the PVDF matrix being low. The absence of significant agglomeration indicated that the TiO₂ nanoparticles were evenly distributed throughout the nanocomposite membrane.

In the cross-sectional images presented in Fig. 6(a)–(f), various finger-like structures were observed within the membrane upper layer, followed by a highly porous support layer resembling a honeycomb structure. This structural configuration resulted in an asymmetrical membrane structure with different pore sizes and porosities, as displayed in Table 2. The formation of these structural features was influenced by the inflow of non-solvent into the membrane during the phase inversion process, affecting their demixing rate.[60–62] Taking into account the incorporation of 4 wt% hydrophilic nanocellulose greatly improved the performance of the developed membrane, especially in terms of enhancing the phase inversion rate and water permeation in contrast to a pristine membrane.[63,64] Numerous studies have emphasized the advantages of nanocellulose in endowing an abundance of –OH functional groups in membrane systems.[11,65–67] This provision of –OH functional groups has been shown to result in an enhancement of membrane water affinity.[68,69] The inclusion of nanocellulose as a reinforcing filler in polymer membrane systems effectively minimized fouling issues associated with hydrophobic foulants on the membrane.[70,71] Moreover, the incorporation of hydrophilic nanocellulose also facilitated rapid non-solvent diffusion into the cast membrane during the solidification process, which caused the appearance of two distinct macrovoids with varying shapes and sizes followed by microvoids underneath as displayed in Fig. 6(a) with a low total membrane porosity of 76.07% compared to others as reported in Table 2. Although this finding contributed to a favorable non-solvent diffusivity outcome, it also caused the formation of a complex membrane network comprising straight finger-like structures as well as shrinkage and irregularly slanted

Table 2 Characteristics of the PVDF/NC and PVDF/NC/TiO$_2$ nanocomposite membranes

Sample	Mean pore size (μm)	Porosity (%)	Average thickness (μm)
S0-PVDF/NC	$4.88 \times 10^{-3} \pm 0.05$	76.07 ± 3.68	4.433×10^{-8}
S1-PVDF/NC/TiO$_2$	$4.98 \times 10^{-3} \pm 0.07$	76.59 ± 4.67	4.133×10^{-8}
S2-PVDF/NC/TiO$_2$	$4.73 \times 10^{-3} \pm 0.03$	77.84 ± 1.05	4.633×10^{-8}
S3-PVDF/NC/TiO$_2$	$4.70 \times 10^{-3} \pm 0.05$	79.68 ± 0.65	4.433×10^{-8}
S4-PVDF/NC/TiO$_2$	$4.79 \times 10^{-3} \pm 0.06$	80.15 ± 2.38	4.633×10^{-8}
S5-PVDF/NC/TiO$_2$	$4.93 \times 10^{-3} \pm 0.04$	83.09 ± 0.89	4.433×10^{-8}

macrovoids. Such slanted macrovoid structures formed as a consequence of the non-uniform evaporation which induced differential expansion.[72] This issue hindered water permeation through the membrane by creating a barrier to water passage and somehow caused fouling. As a result, the incorporation of varying percentages of TiO$_2$ loading into PVDF/NC nanocomposite membrane systems was considered to address this concern. The introduction of TiO$_2$ nanoparticles offered photocatalytic properties and quantum-confined superfluid (QSF) channels within the PVDF/NC/TiO$_2$ matrix.[73]

Different pore configurations were observed upon incorporating varying percentages of TiO$_2$ loadings ranging from 1 wt% to 5 wt% into the nanocomposite membrane system. In particular, the addition of 1 wt% TiO$_2$ in the S1-PVDF/NC/TiO$_2$ as shown in Fig. 6(b) has notably elongated the finger-like pore formation with the absence of slanted macrovoid structures within the nanocomposite membrane. The addition of these hydrophilic inorganic nanoparticles has reinforced the membrane structure by increasing the porosity of the membrane from 76.07% to 76.59% as well as enhancing its stability.[74] This enhancement was achieved through the homogeneous distribution of TiO$_2$ nanoparticles within the membrane matrix which allowed adjustment of the pore structure by forming numerous empty voids on the membrane. These voids potentially enhance the adsorption of contaminants during the membrane application. The study observed that increasing the TiO$_2$ loadings further enlarged both the width and size of the finger-like pore channels as shown in Fig. 5(c)–(f), respectively. This observation was attributed to the increase in the demixing rate, which subsequently improved the structural porosity of the respective membrane as documented in Table 2. The effect of incorporating both nanocellulose and TiO$_2$ nanoparticles has imparted various benefits, making them suitable candidates for diverse wastewater treatment applications.

The notable advantage attributed to their compatibility was the enhanced homogeneity in dispersion, which resulted in improved pore channel development.[75] As observed in the cross-sectional images of the PVDF/NC/TiO$_2$ nanocomposite membranes in Fig. 6, the confirmation of uniform distribution of nanocellulose and TiO$_2$ nanoparticles within the PVDF matrix indicated the absence of nanoparticle agglomeration. The uniform dispersion of these nanoparticles facilitated the consistent development of finger-like pore structures due to the homogeneous exchange rate of DMAc solvent and non-solvent. Additionally, the inclusion of LiCl into the dope solution also synergistically enhanced the inflow of non-solvent into the membrane system during the solidification process as it aided

in developing additional pores in the membrane structure.[58,59] The observed result aligned with previous literature findings, which also showed the development of porous membranes with large cavities on their cross-sectional images when LiCl was incorporated during the membrane development phase.[76] Moreover, the optimal concentration of LiCl can initiate a dynamic interplay between both thermodynamic instability and kinetic effect factors during membrane solidification.[59,76,77] LiCl was highly soluble in DMAc solvent and upon immersion of the casted nanocomposite membrane in the coagulation bath containing non-solvent, an instantaneous liquid–liquid demixing process occurred in which both DMAc solvent and LiCl were rapidly removed from the membrane system.

However, it is important to highlight that the addition of TiO$_2$ loadings was beneficial only up to a certain percentage limit, as beyond this could lead to the development of distorted pores which negatively affect the membrane performance.[33,34,78] This scenario was evident in Fig. 6(f), where numerous distorted macrovoid pores were observed attributed to the increase in dope solution viscosity. The increase in dope solution viscosity was due to the addition of 5 wt% of TiO$_2$ to the S5-PVDF/NC/TiO$_2$ nanocomposite membrane, which caused agglomeration of TiO$_2$ due to the increased ratio of solute-to-solvent, and the formation of numerous open pores on its surface. Consequently, the increase in dope solution viscosity led to a noticeable delay in the demixing process of the solvent and non-solvent exchange rate.[79,80] This delay significantly influenced both the thermodynamic and kinetic parameters as the time taken was prolonged for pore formation.[81] The extended exposure of the casted membrane to the non-solvent caused pore growth and nucleation on the membrane surface which further impacted the physical properties of the membrane, particularly its morphology and thickness.

The elemental composition analysis shown in Table 3 provided additional confirmation of the elements present on the surface of the nanocomposite membrane. Based on the data analysis, all samples recorded the highest elemental percentages of carbon (C) and fluorine (F) as they were the major elements in PVDF polymer.[82,83] This result provided valuable insights into the correlation between the C and F elemental composition with the identified C–F bond in the FTIR analysis. The analysis showed that the incorporation of TiO$_2$ loadings into the nanocomposite membrane increased proportionally with the elemental composition of titanium (Ti) and oxygen (O). However, the highest increment in percentages of Ti and O elements in S5-PVDF/NC/TiO$_2$ resulted from the poor distribution of TiO$_2$ nanoparticles as displayed in Fig. 3(k) of the FESEM result.

Table 3 EDX analysis of the controlled PVDF/NC and PVDF/NC/TiO$_2$ nanocomposite membranes with varying TiO$_2$ compositions

Membrane sample	Elemental (%)			
	C	O	F	Ti
S0-PVDF/NC	57.43 ± 0.03	4.18 ± 0.02	38.39 ± 0.04	—
S1-PVDF/NC/TiO$_2$	55.10 ± 0.02	5.28 ± 0.02	38.19 ± 0.04	1.43 ± 0.01
S2-PVDF/NC/TiO$_2$	53.93 ± 0.02	5.68 ± 0.02	37.50 ± 0.04	2.89 ± 0.01
S3-PVDF/NC/TiO$_2$	53.57 ± 0.02	5.53 ± 0.02	38.00 ± 0.04	2.90 ± 0.01
S4-PVDF/NC/TiO$_2$	53.23 ± 0.02	5.30 ± 0.02	38.55 ± 0.04	2.92 ± 0.01
S5-PVDF/NC/TiO$_2$	52.57 ± 0.02	6.85 ± 0.02	36.65 ± 0.04	3.93 ± 0.01

3.3 Crystallographic analysis of the nanocomposite membrane

The displayed graphical representation in Fig. 7 showed a comparative visualization of the crystallinity and crystallographic structures of the PVDF/NC nanocomposite membrane and the impact of varying loading percentages of TiO$_2$ on the XRD profile of the PVDF/NC/TiO$_2$ nanocomposite membrane. Based on the literature, PVDF is classified as a semicrystalline polymer consisting of multiple crystalline phases α, β, γ and δ.[84,85] Among these, the α and β phases are the most commonly detected in studies related to pristine PVDF membranes, which typically have XRD diffraction peaks at angles of approximately 18° and 20°.[86–89] The analysis in Fig. 7 showed that the addition of nanocellulose resulted in the prominence of the β-phase as evidenced by the XRD profile of the PVDF/NC nanocomposite membrane. The crystallinity of the nanocellulose was improved with the addition of LiCl in the membrane system during the dope solution preparation.[90] The XRD diffraction pattern of the controlled membrane PVDF/NC revealed a distinct peak at 20.43°, which corresponded to the (110) crystal planes of the PVDF β-phase. An additional peak appeared in samples incorporating TiO$_2$ nanoparticles, which corresponded to the reflections at 25.12°, 25.15° and 25.13°. These identified peaks confirmed the existence of the TiO$_2$ anatase phase with the (101) crystal plane that contributed to the antifouling properties in the developed PVDF/NC/TiO$_2$ membrane.[84]

Based on the observations, the increase in TiO$_2$ loadings resulted in an intense diffraction peak intensity at 25°, which indicated an improved interaction between the functional groups of PVDF, nanocellulose and TiO$_2$ associated with its deposition. In correlation with the discussion, the crystallinity percentages of the sample increased proportionally with the rising loadings of TiO$_2$. For instance, the inclusion of 1 wt% of TiO$_2$ in the S1-PVDF/NC/TiO$_2$ system enhanced the crystallinity percentages from 16.86% to 26.48%, followed by 41.92% for the sample S5-PVDF/NC/TiO$_2$. Among all nanocomposite samples, S5-PVDF/NC/TiO$_2$ revealed the highest crystallinity in the membrane, which indicated a more structured and ordered sample representation. This was attributed to the abundance of TiO$_2$ nanoparticles on the membrane surface which affected the phase inversion dynamics during the fabrication process that led to a more pronounced rearrangement of the PVDF chains. According to the literature, an increase in the crystallinity index of a membrane has the potential to improve its performance in various applications.[40,91,92] Improved crystallinity fosters strong interfacial interactions within the membrane matrix, which demonstrates excellent pore-forming capabilities.[65] In this study, it was observed that the increase in crystallinity index corresponded to an increase in the average crystallite size. However, this correlation was complex as it could vary depending on several factors as some studies have found that the crystallinity index was independent of crystallite size.[93] The average crystallite size was analyzed using the Debye Scherrer equation as shown in eqn (2).

3.5 Performance evaluations and comparative analyses of the nanocomposite membrane

3.5.1 Water flux analysis of the nanocomposite membranes. Water flux was examined to evaluate the permeability
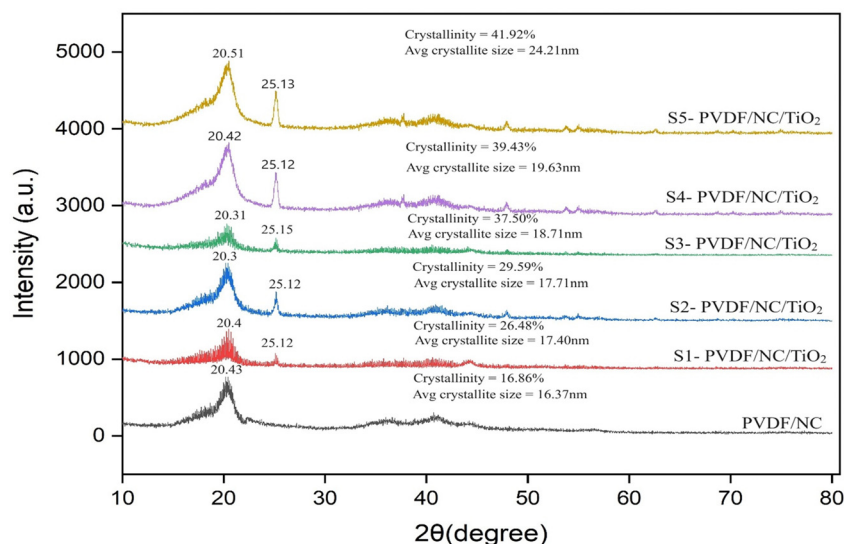
Fig. 7 XRD analysis of PVDF/NC and PVDF/NC/TiO$_2$ nanocomposite membranes with varying TiO$_2$ loading percentages.
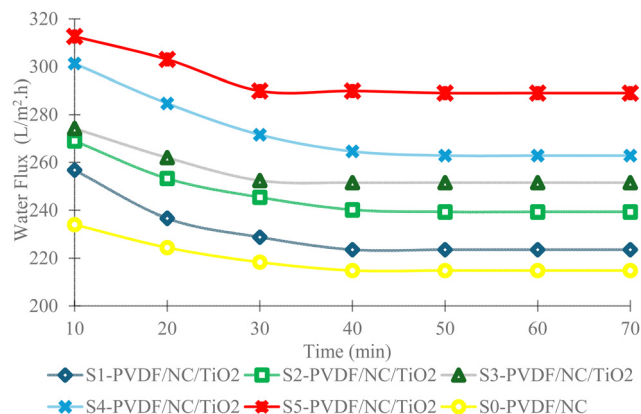
Fig. 8 Comparative water flux analysis of PVDF/NC and PVDF/NC/TiO$_2$ nanocomposite membranes across varied TiO$_2$ loading percentages.

rate through novel fabricated nanocomposite membranes by measuring the amount of permeate collected per membrane surface area over time at 1 bar while observing the effect of varying the TiO$_2$ nanoparticle loadings in the membrane system. Based on the analysis presented in Fig. 8, the incorporation of TiO$_2$ into the nanocomposite membrane system significantly improved water permeation in contrast to the S0-PVDF/NC membrane. The analysis revealed a proportional relationship between TiO$_2$ loading incorporated into the (S1–S5)-PVDF/NC/TiO$_2$ nanocomposite membrane and the water permeation flux passed through the membrane. This finding showed a promising outcome, as the addition of TiO$_2$ nanoparticles had contributed to the formation of a homogeneous nanocomposite membrane structure with enhanced properties and productivity. By considering the addition of 1 wt% TiO$_2$ nanoparticles to the PVDF/NC matrix, the water permeation of the respective nanocomposite membrane increased from 234.06 L m^{-2} h^{-1} to 256.76 L m^{-2} h^{-1} within the first 10 minutes. This enhancement was due to the development of numerous elongated finger-like pore channels within the S1-PVDF/NC/TiO$_2$ nanocomposite membrane as displayed by the FESEM result, which allowed more water to permeate through it. Further enhancement of the water permeation flux was noticed with the additional amount of TiO$_2$ nanoparticles to 268.99 L m^{-2} h^{-1} (2 wt% TiO$_2$), 274.23 L m^{-2} h^{-1} (3 wt% TiO$_2$), 301.31 L m^{-2} h^{-1} (4 wt% TiO$_2$) and 312.66 L m^{-2} h^{-1} (5 wt% TiO$_2$), respectively. Numerous studies have supported the current finding, which distinguished that the presence of different hydrophilic additives initiated a synergistic effect in the pristine PVDF membrane, enhancing the membrane hydrophilicity behavior and consequently improving flux rates and antifouling performance.[74,94,95] This outcome aligned with the expectations which correlated to the findings presented in Table 2. The porosity percentage of the nanocomposite membrane showed improvement, progressing from 76.07% for PVDF/NC to 76.59% (S1-PVDF/NC/TiO$_2$), 77.84% (S2-PVDF/NC/TiO$_2$), 79.68% (S3-PVDF/NC/TiO$_2$), 80.15% (S4-PVDF/NC/TiO$_2$) and reaching 83.09% for sample S5-PVDF/NC/TiO$_2$. The analysis also revealed that the system reached a steady flux state within a 30 to 40-minute

timeframe with the reduction not exceeding 15% from the initial values. Based on studies, this finding is typically associated with an ultrafiltration membrane compared to a microfiltration membrane.[96,97]

It was also found that the rate of water permeation flux by the developed PVDF/NC/TiO$_2$ nanocomposite membranes was comparable to the existing literature. The water permeation flux in the present study exceeded that reported for cellulose acetate/TiO$_2$ (CA-TiO$_2$) membrane systems with 17.5 wt% polymer and 20 wt% TiO$_2$ compositions, despite these material compositions being higher than the designed compositions used in this study. The result revealed that the maximum achieved water permeation rate was 47.42 L m^{-2} h^{-1}.[98] Another study examined the impact of incorporating two similar hydrophilic additives, namely nanocellulose and TiO$_2$ nanoparticles using silane-modified TiO$_2$ nanoparticles, which resulted in a permeate flux of approximately 2.5 L m^{-2} h^{-1}, lower than that of the present study.[34] Based on the literature, the low water permeation rate was ascribed to the modification, which initiated pore blocking and increased resistance in mass transfer. However, the developed membrane exhibited an outstanding salt removal performance as it was able to remove 97.7%. Moreover, another study recorded similar water flux rates when incorporating chitosan cellulose and 30 wt% TiO$_2$ nanoparticles into the PVDF membrane.[99] The introduction of these two hydrophilic additives enhanced the capillary-driven water volume to 6.39 L due to the formation of nanoporous structures within the membrane which consequently caused a high water permeation rate.

3.5.2 MB dye removal analysis of nanocomposite membranes. In order to comprehensively evaluate the separation efficacy of the fabricated PVDF/NC and PVDF/NC/TiO$_2$ nanocomposite membranes, a series of MB dye removal tests were conducted with an initial concentration of 1 ppm. Each sample was meticulously repeated five times to obtain the average values as presented by the line graph in Fig. 9. Upon analysis, it was observed that the result obtained for dye removal flux was lower than the water flux analysis with the highest dye removal flux achieved by sample S3-PVDF/NC/TiO$_2$ (70 L m^{-2} h^{-1}),
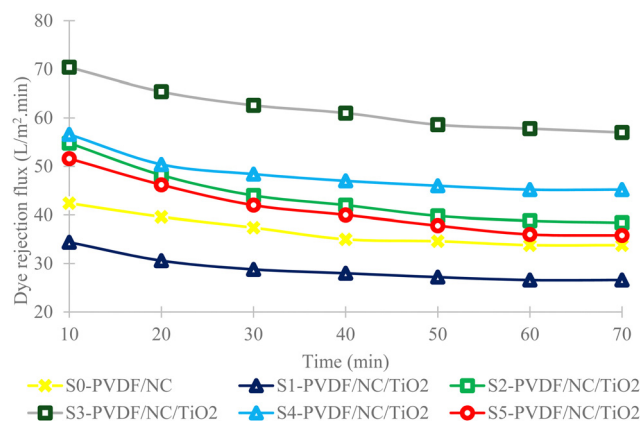

Fig. 9 Comparative dye removal flux analysis of PVDF/NC and PVDF/NC/TiO$_2$ nanocomposite membranes across varied TiO$_2$ loading percentages.
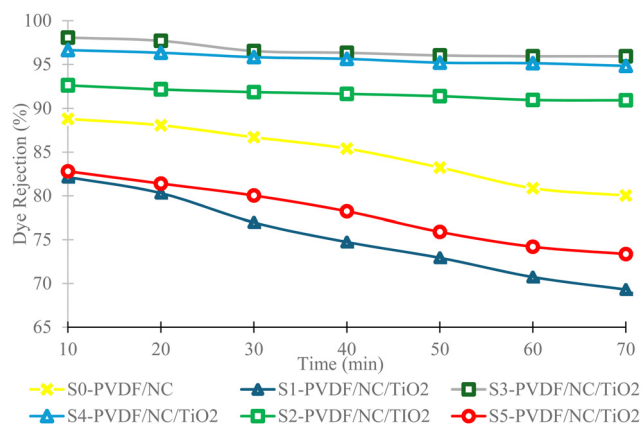
Fig. 10 Analysis of MB dye removal percentages using PVDF/NC and PVDF/NC/TiO$_2$ nanocomposite membranes across varied TiO$_2$ loading percentages.

followed by S4-PVDF/NC/TiO$_2$ (56 L m^{-2} h^{-1}), S2-PVDF/NC/TiO$_2$ (54 L m^{-2} h^{-1}), S5-PVDF/NC/TiO$_2$ (51 L m^{-2} h^{-1}), S0-PVDF/NC/TiO$_2$ (42 L m^{-2} h^{-1}) and S1-PVDF/NC/TiO$_2$ (34 L m^{-2} h^{-1}) in the first 10-minute run. This result was correlated with the MB removal percentages shown in Fig. 10 and corresponded to the dye color variations shown in Table 4. In the first 10-minute run, S3-PVDF/NC/TiO$_2$ demonstrated exceptional performance with a remarkable MB removal percentage of 98%. The dye removal rate was significantly higher than that of S1-PVDF/NC/TiO$_2$ and S2-PVDF/NC/TiO$_2$, with removal percentages of 82% and 92%, respectively. Impressively, this high removal rate of S3-PVDF/NC/TiO$_2$ persisted even after a 30-minute run, demonstrating the nanocomposite membrane effectiveness over time. The nanocomposite initially rejected 98% of MB dye and only slightly decreased to 96% after a 70-minute investigation. This consistent trend underscored the effectiveness of the membrane in the removal of dye pollutants owing to its antifouling properties.

Based on a comparative analysis, the finding from S3-PVDF/NC/TiO$_2$ revealed a slightly higher removal rate compared to the result of using modified PVDF with 2,2,6,6-tetramethyl-piperidine-11-oxyl-oxidized cellulose nanofiber (TCNF-PVDF), which exhibited a removal percentage of 95.1%.[65] According to the researchers, the introduction of TNCF aided in enhancing the hydrophilic behavior of the membrane as well as imparting more surface charges in the membrane matrix. This statement supported the present finding, where increasing the dosage of TiO$_2$ nanoparticle loadings to 3 wt% as well as the presence of nanocellulose significantly contributed to the

Table 4 Membrane illustration and dye collection dynamics before and after photocatalytic treatment

Sample	Membrane condition pre-photocatalytic treatment	Dye collection over time	Membrane condition post-photocatalytic treatment
S0-PVDF/NC			
S1-PVDF/NC/TiO$_2$			
S2-PVDF/NC/TiO$_2$			
S3-PVDF/NC/TiO$_2$			
S4-PVDF/NC/TiO$_2$			
S5-PVDF/NC/TiO$_2$			

improvement of surface functionalization in the nanocomposite membrane due to the abundance of hydroxyl (–OH) functional groups.[100] These hydroxyl functional groups facilitated the adsorption of cationic organic polar pollutants, particularly MB dye. According to the literature, membrane surface charge was highlighted as one of the important parameters to consider for the selective removal of pollutants.[101–103] For instance, increasing the dosage of TiO_2 nanoparticles imparted more negative charges on the surface of the nanocomposite membrane, which in turn improved the membrane hydrophilicity behavior. This surface modification resulted in a higher adsorption percentage of cationic MB dye upon contact with the nanocomposite membrane due to the strong electrostatic attraction and π–π stacking interaction between the MB dye molecules.[104] The adsorption was further enhanced with the presence of hydrogen bonding in the system.[100]

Moreover, the inclusion of nanomaterials themselves characterized by a high surface area led to increased adsorption capacity on the active sites of the material.[73,78,105–107] The presence of nanocellulose provided more available unoccupied sites for capturing MB pollutants through van der Waals interaction, which enhanced the movement and distribution of MB dye molecules to the surface of the respective nanocomposite membrane, thereby improving the overall performance.[11] Due to the high MB removal percentage by S3-PVDF/NC/TiO_2, the collected MB dye permeates as displayed in Table 4 exhibited clearer color variation compared to the controlled sample S0-PVDF/NC, which had a removal percentage of only 88.8%. Based on the observation, it can be deduced that the inclusion of both nanocellulose and TiO_2 nanoparticles, two distinct hydrophilic additives, exceeded the impact of incorporating a single hydrophilic additive. This analysis was also acknowledged by other researchers in their respective studies.[108,109] The synergistic effect of this combination facilitated enhanced pore development which resulted in numerous additional void generations.[108] These voids provided more vacancies for the adsorption of MB dye pollutants. A similar finding was reported by other researchers, indicating that the presence of numerous voids enhanced the capacity for capturing and removing pollutants from the subjected wastewater, while also bolstering its resistance to fouling.[34,108] Apart from that, another factor that influenced the efficiency of MB dye removal was the physicochemical properties of the nanocomposite membrane. The size of the developed pores played a crucial role in selective filtration and separation processes by determining which molecules could pass through while restricting larger molecules. Based on the pore size analysis from the previous section, S0-PVDF/NC exhibited a mean pore size of 4.88×10^{-3} μm, slightly larger than that of S3-PVDF/TiO_2 (4.70×10^{-3} μm). The larger pore size of S0-PVDF/NC permitted some MB dye pollutants to pass through the membrane as the size of the MB dye pollutants was smaller than the respective nanocomposite pore size, thereby reducing MB dye removal efficiency. This finding is supported by the existing literature, which indicates that the selectivity of the membrane is contingent upon both pore and pollutant sizes.[110]

Comparing the dye removal flux results of samples S5-PVDF/NC/TiO_2 and S0-PVDF/NC, S5-PVDF/NC/TiO_2 favored a high dye removal flux possibly due to the formation of larger pore size of 4.93×10^{-3} μm. However, the dye removal percentage of this sample was lower than that of S0-PVDF/NC, initially rejecting only 82.8% while the S0-PVDF/NC removal efficiency achieved 88.8%. In conjunction with the discussion related to the pore size, a larger pore size could potentially lead to intermediary pore blockage. A study stated that larger pore size entrapped pollutants of similar size and blocked the membrane pores as they deposited within the pores, forming pollutant accumulations that consequently caused membrane fouling.[111] This problem resulted in a rapid reduction in MB dye removal flux as demonstrated by samples S0-PVDF/NC, S5-PVDF/NC/TiO_2 and S1-PVDF/NC/TiO_2 in Fig. 9.[112] In this study, the incorporation of TiO_2 nanoparticles into the nanocomposite membrane system aided in addressing membrane fouling issues, which typically increased the membrane efficiency and overall lifespan.

3.5.3 Photocatalytic and antifouling properties analysis of nanocomposite membranes. Based on the membrane visualization presented in Table 4 before and after photocatalytic treatment, it was evident that the appearance showed a direct relationship between the rate of photodegradation and the loading percentages of TiO_2 nanoparticles in the nanocomposite membrane. The incorporation of TiO_2 nanoparticles into membrane technology enhanced membrane fouling mitigation and reduced the necessity for backwashing as this approach often encountered difficulties in backwash recovery, especially concerning productivity.[113,114] According to other researchers, the inclusion of TiO_2 nanoparticles into their fabricated TiO_2/PVA PVDF membrane assisted in degrading the substantial accumulation of protein molecules present on the surface of their membrane, known as the fouling cake.[60] This contrasted with the performance of their pristine PVDF membrane. Similar to the current investigation, the absence of TiO_2 nanoparticles in the membrane system did not lead to any noticeable difference in the appearance of MB dye pollutants on the S0-PVDF/NC membrane surface.[115] However, interestingly, the introduction of a small quantity of TiO_2 nanoparticles seemed to result in some degradation of MB pollutants. Based on the study, the inclusion of 1 wt% TiO_2 in the PVDF/NC nanocomposite membrane subtly removed MB pollutants under UV light irradiation.

The elevation in the loading percentages of TiO_2 nanoparticles further increased the decolorization of MB molecules adhered to the surface of the nanocomposite membrane.[116] This improvement was achieved in the presence of UV light irradiation, where TiO_2 which consists of an abundance of active sites absorbed photons and triggered the generation of electron–hole pairs.[117] The excited photogenerated electrons and holes participated in the redox reaction with the adsorbed MB dye pollutants. The redox reaction caused the free electrons (e^-) to react with oxygen (O_2) molecules and formed superoxide radical anions (O_2^-), while the holes (h^+) acted as oxidizing agents and reacted with water molecules (H_2O) and hydroxide

ions (OH^-) to form hydroxyl radicals $(OH^{\bullet})$. According to studies, superoxide radicals also potentially contributed to the generation of hydrogen peroxide (H_2O_2) when reacted with water. The reactive species, including superoxide radicals (O_2^-), hydroxyl radicals (OH^-), hydrogen peroxide (H_2O_2) and oxygen (O_2) played a significant role in the degradation of MB dye pollutants on the surface of the nanocomposite membrane, which resulted in the generation of non-toxic compounds including water (H_2O), carbon dioxide (CO_2) and mineral acids.[117–119]

The antifouling property of the S0-PVDF/NC and (S1–S5)-PVDF/NC/TiO$_2$ nanocomposite membranes, flux recovery rate (FRR), was identified to provide insights into the performance of the nanocomposite membrane after being subjected to the various filtration processes. Based on Fig. 11, the S5-PVDF/NC/TiO$_2$ nanocomposite membrane showed the highest flux recovery rate compared to the others, followed by S4-PVDF/NC/TiO$_2$, S3-PVDF/NC/TiO$_2$, S2-PVDF/NC/TiO$_2$, S1-PVDF/NC/TiO$_2$ and S0-PVDF/NC/TiO$_2$, respectively. Within the first 30-minute run, the recovery flux of all nanocomposite samples showed a rapidly declining trend and then remained consistently linear. The water recovery permeate flux exhibited by the S5-PVDF/NC/TiO$_2$ nanocomposite membrane was approximately $270 \text{ L m}^{-2} \text{ h}^{-1}$ with an FRR of 93.65%, indicating a reduction of 6.35% due to fouling. In comparison, the S4-PVDF/NC/TiO$_2$ nanocomposite membrane recorded a reduction in recovery flux of $245 \text{ L m}^{-2} \text{ h}^{-1}$, while the S3-PVDF/NC/TiO$_2$ and S2-PVDF/NC/TiO$_2$ membranes recorded fluxes of $225 \text{ L m}^{-2} \text{ h}^{-1}$ and $214 \text{ L m}^{-2} \text{ h}^{-1}$. The S1-PVDF/NC/TiO$_2$ nanocomposite membrane exhibited a recovery flux of $176.42 \text{ L m}^{-2} \text{ h}^{-1}$ and the lowest recovery flux was recorded by S0-PVDF/NC with a permeate flux of $151 \text{ L m}^{-2} \text{ h}^{-1}$. The corresponding FRR percentages for these membranes after being subjected to photocatalytic activity were comparably high compared to other results reported by other researchers, with values of 93.35%, 89.78%, 89.58%, 78.9%, and 70.32%, respectively. In general, higher percentages of FRR indicated better self-cleaning and antifouling properties.[108,120]
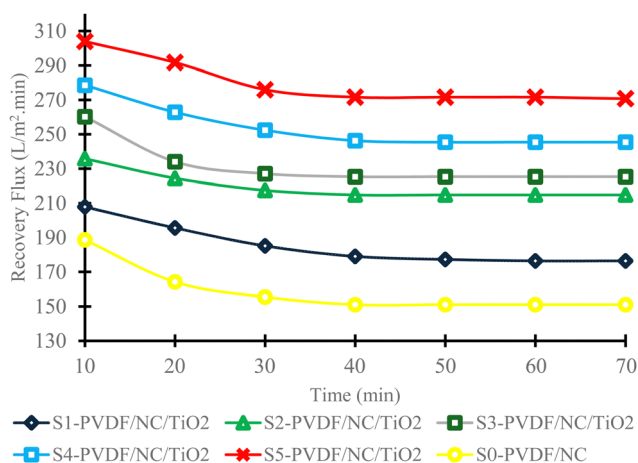

Fig. 11 Recovery water flux rates of nanocomposite membranes post-photocatalytic activity.

The synergistic effect of combining $Mg(OH)_2$ with rice husk silica for humic acid (HA) removal presented a substantial finding with an FRR percentage of 84.07% compared to the membrane with a single additive showing an FRR of 30.87%.[108] This observation effectively supported the current findings regarding the outstanding antifouling properties when incorporating both NC and TiO$_2$ to boost their synergies in resisting fouling, thereby maintaining longevity in practical applications. A study showed that the antifouling properties of a PVDF membrane were improved by incorporating commercial cellulose nanocrystals (CNC), which imparted more active sites on the membrane.[90] The study reported an FRR of $<85\%$ with a high permeation flux under a 100 kPa operating pressure. The mean pore size of the subjected membrane was found to be 30 nm, larger than the mean pore size of the fabricated S0-PVDF/NC and (S1–S5)-PVDF/NC/TiO$_2$ nanocomposite membranes. However, in comparison with the present study, the FRR result of the PVDF membrane modified with commercial cellulose nanocrystals (CNCs) was still low. Conversely, another study focused on chemical modification to improve membrane hydrophilicity and antifouling properties *via* polyethyleneimine (PEI) amination and poly(methyl vinyl ether-*alt*-maleic anhydride) modification.[121] The result surpassed others, achieving an FRR of 97% with bovine serum albumin (BSA) rejection. However, the complexity and potential toxicity risk associated with high concentrations of PEI may pose difficulties to practical implementation in wastewater treatment. Based on the overall findings gleaned from published studies related to pristine PVDF membrane and PVDF membrane modified with various types of hydrophilic additives, a notable observation was made where most of the studies recorded FRRs of less than 90% and some lacked a comprehensive evaluation of the antifouling properties.[84,90,108,122] Instead, the predominant focus of these studies was directly on membrane morphology, composition compatibility and filtration performance.

4. Conclusion

This study elucidates the nuanced interactions and enhancements in PVDF/NC and PVDF/NC/TiO$_2$ nanocomposite membranes, revealing significant advancements in membrane technology for wastewater treatment. The integration of NC and TiO$_2$ nanoparticles within the PVDF matrix significantly improves the structural, mechanical, and functional properties of the membranes. The FTIR analysis confirms the presence of functional groups that are pivotal in enhancing the interaction between the PVDF matrix and the nanocomposite additives. These interactions are further evidenced by XRD results, which show an increase in crystallinity particularly evident in the β-phase of PVDF, correlating with enhanced mechanical stability and function. FESEM images provided detailed insights into the morphological changes which revealed that lower TiO$_2$ loadings resulted in well-dispersed nanoparticles, contributing to the formation of a more porous and permeable membrane structure. In contrast, higher TiO$_2$ loadings that exceeded the

Paper

optimal limits led to agglomeration issues as evidenced in the S5-PVDF/NC/TiO$_2$ membrane. The results deduce that optimized loading of TiO$_2$ not only prevents pore blockage but also promotes a high degree of crystallinity and pore formation, directly enhancing the filtration efficiency. This is particularly evident in the performance of the S3-PVDF/NC/TiO$_2$, where the inclusion of only 3 wt% of TiO$_2$ results in an outperforming MB dye removal percentage of 98%, with a comparably high water permeation flux of 274.23 L m^{-2} h^{-1} and FRR of 89.78%. The synthesis of PVDF/NC/TiO$_2$ nanocomposite membranes thus presents a robust approach to addressing the challenges of membrane fouling and efficiency in wastewater treatment applications. The dual incorporation of NC and TiO$_2$ within the PVDF matrix not only leverages the intrinsic properties of each component but also synergizes their effects, thereby enhancing the overall performance of the membrane system. This study contributes to the ongoing development of advanced membrane technologies, offering promising avenues for sustainable and efficient environmental remediation solutions.

Abbreviations

NC	Nanocellulose
FTIR	Fourier transform infrared
ATR-FTIR	Attenuated total reflectance-Fourier transform infrared
FESEM	Field emission scanning electron microscopy
XRD	X-ray crystallography
EDX	Energy-dispersive X-ray
UV-Vis	Ultraviolet-visible spectroscopy
PI	Process intensification
MB	Methylene blue
CAS	Chemical abstracts service
DI	Deionized water
UNIMAS	Universiti Malaysia Sarawak
NIPS	Non-solvent-induced phase separation
PVDF/NC	Polyvinylidene fluoride/nanocellulose
PVDF/NC/TiO$_2$	Polyvinylidene fluoride/nanocellulose/titanium dioxide
S0	Sample 0
S1	Sample 1
S2	Sample 2
S3	Sample 3
S4	Sample 4
S5	Sample 5
ΔT	Change of filtration time (h)
ΔP	Change of pressure applied (Pa)
J_W	Pure water permeation flux (L m^{-2} h^{-1})
V	Permeate volume (m^3)
A	Effective area of membrane (m^2)
ppm	Parts per million
J_{MB}	Permeate methylene blue
J_{W2}	Pure water permeation flux after photocatalytic activity
R	Dye rejection ratio
C_f	Final concentration
C_i	Initial concentration
UV	Ultraviolet
FRR	Flux recovery ratio
ASTM	American society for testing and materials
CH	Crystalline index
D	Debye Scherrer
K	Debye Scherrer constant
FWHM	Full width at half maximum
ε	Membrane porosity
W_{wm}	Weight of wet membrane (g)
W_{dm}	Weight of dry membrane (g)
ρ_{water}	Water density (g cm^{-3})
ρ_{PVDF}	Polyvinylidene fluoride density (g cm^{-3})
η	Water viscosity
l	Membrane thickness
Q	Volume of water permeation (m^3 s^{-1})

Author contributions

Md Rezaur Rahman: editor and draft preparation. Anthonette James: experiment and draft preparation. Khairul Anwar Mohamed Said: editor. Murtala Namakka: experiment. Mayeen Uddin Khandaker: experiment XRD. Woo Haw Jiunn: analysis of XRD. Jehan Y. Al-Humaidi: editor and funder. Raed H. Althomali: editor and funder. Mohammed Muzibur Rahman: editor and funder.

Data availability

Data will be available on request.

Conflicts of interest

The authors declare no conflict of interest.

Acknowledgements

References

1 J. Cai, D. Zhao and O. Varis, Match Words with Deeds: Curbing Water Risk with the Sustainable Development Goal 6 Index, *J. Cleaner Prod.*, 2021, **318**, 128509, DOI: **10.1016/j.jclepro.2021.128509**.

2 S. Mondal and D. Palit, Challenges in Natural Resource Management for Ecological Sustainability, *Natural Resources Conservation and Advances for Sustainability*, Elsevier, 2022, pp. 29–59, DOI: **10.1016/B978-0-12-822976-7.00004-1**.

3 B. Ramesh, A. Saravanan, P. Senthil Kumar, P. R. Yaashikaa, P. Thamarai, A. Shaji and G. Rangasamy, A Review on Algae Biosorption for the Removal of Hazardous Pollutants from Wastewater: Limiting Factors, Prospects and Recommendations, *Environ. Pollut.*, 2023, **327**, 121572, DOI: **10.1016/j.envpol.2023.121572**.

4 R. Al-Tohamy, S. S. Ali, F. Li, K. M. Okasha, Y. A.-G. Mahmoud, T. Elsamahy, H. Jiao, Y. Fu and J. Sun, A Critical Review on the Treatment of Dye-Containing Wastewater: Ecotoxicological and Health Concerns of Textile Dyes and Possible Remediation Approaches for Environmental Safety, *Ecotoxicol. Environ. Saf.*, 2022, **231**, 113160, DOI: **10.1016/j.ecoenv.2021.113160**.

5 A. P. Periyasamy, Recent Advances in the Remediation of Textile-Dye-Containing Wastewater: Prioritizing Human Health and Sustainable Wastewater Treatment, *Sustainability*, 2024, **16**(2), 495, DOI: **10.3390/su16020495**.

6 A. Saravanan, P. Senthil Kumar, S. Jeevanantham, S. Karishma, B. Tajsabreen, P. R. Yaashikaa and B. Reshma, Effective Water/Wastewater Treatment Methodologies for Toxic Pollutants Removal: Processes and Applications towards Sustainable Development, *Chemosphere*, 2021, **280**, 130595, DOI: **10.1016/j.chemosphere.2021.130595**.

7 S. S. Tarun, S. K. Dakshesh and G. Arthanareeswaran, Tuning of Polymeric Membranes to Mitigate Fouling and Removal of Dissolved Compounds for Wastewater Treatment: A Review, *Front. Membr. Sci. Technol.*, 2024, **3**, 1389239, DOI: **10.3389/frmst.2024.1389239**.

8 R. S. Zambare and P. R. Nemade, Polymer Nanocomposite Membranes for Wastewater Treatment, *Handbook of Nanomaterials for Wastewater Treatment*, Elsevier, 2021, pp. 605–672, DOI: **10.1016/B978-0-12-821496-1.00021-0**.

9 H. A. Abbas, K. K. Abbas and A. M. Al-Ghaban, MXene (TiC Tx) Based Nanosheet Photocatalysts for Water Remediation: Challenges and Recent Developments, *Eng. Technol. J.*, 2024, **42**(6), 708–721, DOI: **10.30684/etj.2024.146505.1683**.

10 A. James, M. R. Rahman, K. A. Mohamad Said, D. Kanakaraju, A. Z. Sueraya, K. K. Kuok, M. K. Bin Bakri and M. M. Rahman, A Review of Nanocellulose Modification and Compatibility Barrier for Various Applications, *J. Thermoplast. Compos. Mater.*, 2023, **37**(6), 2149–2199, DOI: **10.1177/08927057231205451**.

11 M. N. Norizan, S. S. Shazleen, A. H. Alias, F. A. Sabaruddin, M. R. M. Asyraf, E. S. Zainudin, N. Abdullah, M. S. Samsudin, S. H. Kamarudin and M. N. F. Norrrahim, Nanocellulose-Based Nanocomposites for Sustainable Applications: A Review, *Nanomaterials*, 2022, **12**(19), 3483, DOI: **10.3390/nano12193483**.

12 T. C. Mokhena, M. J. Mochane, A. Mtibe, S. Sigonya, B. Ntsendwana, E. G. Masibi, L. Sikhwivhilu and T. S. Motsoeneng, Recent Advances on Nanocellulose-Graphene Oxide Composites: A Review, *Cellulose*, 2024, **31**, 7207–7249, DOI: **10.1007/s10570-024-06055-9**.

13 S. Moyo, N. N. Gumbi, L. A. De Kock and E. N. Nxumalo, A Mini-Review of Nanocellulose-Based Nanofiber Membranes Incorporating Carbon Nanomaterials for Dye Wastewater Treatment, *Environ. Nanotechnol., Monit. Manage.*, 2022, **18**, 100714, DOI: **10.1016/j.enmm.2022.100714**.

14 P. A. Nizam, V. Arumughan, A. Baby, M. A. Sunil, D. Pasquini, A. Nzihou, S. Thomas and D. A. Gopakumar, Mechanically Robust Antibacterial Nanopapers through Mixed Dimensional Assembly for Anionic Dye Removal, *J. Polym. Environ.*, 2020, **28**(4), 1279–1291, DOI: **10.1007/s10924-020-01681-3**.

15 Y. Shi, J. Huang, G. Zeng, W. Cheng and J. Hu, Photocatalytic Membrane in Water Purification: Is It Stepping Closer to Be Driven by Visible Light?, *J. Membr. Sci.*, 2019, **584**, 364–392, DOI: **10.1016/j.memsci.2019.04.078**.

16 Y. Liu, H. Liu and Z. Shen, Nanocellulose Based Filtration Membrane in Industrial Waste Water Treatment: A Review, *Materials*, 2021, **14**(18), 5398, DOI: **10.3390/ma14185398**.

17 E. Demirel, B. Zhang, M. Papakyriakou, S. Xia and Y. Chen, Fe$_2$O$_3$ Nanocomposite PVC Membrane with Enhanced Properties and Separation Performance, *J. Membr. Sci.*, 2017, **529**, 170–184, DOI: **10.1016/j.memsci.2017.01.051**.

18 R. R. Abdullah, K. M. Shabeeb, A. B. Alzubaydi, A. Figoli, A. Criscuoli, E. Drioli and Q. F. Alsalhy, Characterization of the Efficiency of Photo-Catalytic Ultrafiltration PES Membrane Modified with Tungsten Oxide in the Removal of Tinzaparin Sodium, *Eng. Technol. J.*, 2022, **40**(12), 1–10, DOI: **10.30684/etj.2022.134070.1219**.

19 O. A. Afolabi and N. Ndou, Synergy of Hybrid Fillers for Emerging Composite and Nanocomposite Materials-a Review, *Polymers*, 2024, **16**(13), 1907, DOI: **10.3390/polym16131907**.

20 D. Aydin, I. H. Gubbuk and M. Ersoz, Recent Advances and Applications of Nanostructured Membranes in Water Purification, *Turk. J. Chem.*, 2024, **48**(1), 1–20, DOI: **10.55730/1300-0527.3635**.

21 A. Nain, A. Sangili, S.-R. Hu, C.-H. Chen, Y.-L. Chen and H.-T. Chang, Recent Progress in Nanomaterial-Functionalized Membranes for Removal of Pollutants, *iScience*, 2022, **25**(7), 104616, DOI: **10.1016/j.isci.2022.104616**.

22 A. Yusuf, A. Sodiq, A. Giwa, J. Eke, O. Pikuda, G. De Luca, J. L. Di Salvo and S. Chakraborty, A Review of Emerging Trends in Membrane Science and Technology for Sustainable Water Treatment, *J. Cleaner Prod.*, 2020, **266**, 121867, DOI: **10.1016/j.jclepro.2020.121867**.

23 E. A. López-Guajardo, F. Delgado-Licona, A. J. Álvarez, K. D. P. Nigam, A. Montesinos-Castellanos and R. Morales-Menendez, Process Intensification 4.0: A New Approach for Attaining New, Sustainable and Circular Processes Enabled by Machine Learning, *Chem. Eng. Process.*, 2022, **180**, 108671, DOI: **10.1016/j.cep.2021.108671**.

24 C. Ramírez-Márquez, M. M. Al-Thubaiti, M. Martín, M. M. El-Halwagi and J. M. Ponce-Ortega, Processes Intensification for Sustainability: Prospects and Opportunities,

Ind. Eng. Chem. Res., 2023, **62**(6), 2428–2443, DOI: **10.1021/acs.iecr.2c04305**.

25 B. A. Patel and C. S. Pereira, Process Intensification at Scale: An Industrial Perspective, *Chem. Eng. Process.*, 2022, **181**, 109098, DOI: **10.1016/j.cep.2022.109098**.

26 S. F. Ahmed, F. Mehejabin, A. Momtahin, N. Tasannum, N. T. Faria, M. Mofijur, A. T. Hoang, D.-V. N. Vo and T. M. I. Mahlia, Strategies to Improve Membrane Performance in Wastewater Treatment, *Chemosphere*, 2022, **306**, 135527, DOI: **10.1016/j.chemosphere.2022.135527**.

27 Y. Davoodbeygi, M. Askari, E. Salehi and S. Kheirieh, A Review on Hybrid Membrane-Adsorption Systems for Intensified Water and Wastewater Treatment: Process Configurations, Separation Targets, and Materials Applied, *J. Environ. Manage.*, 2023, **335**, 117577, DOI: **10.1016/j.jenvman.2023.117577**.

28 E. Kavitha, E. Poonguzhali, D. Nanditha, A. Kapoor, G. Arthanareeswaran and S. Prabhakar, Current Status and Future Prospects of Membrane Separation Processes for Value Recovery from Wastewater, *Chemosphere*, 2022, **291**, 132690, DOI: **10.1016/j.chemosphere.2021.132690**.

29 N. Nasrollahi, L. Ghalamchi, V. Vatanpour and A. Khataee, Photocatalytic-Membrane Technology: A Critical Review for Membrane Fouling Mitigation, *J. Ind. Eng. Chem.*, 2021, **93**, 101–116, DOI: **10.1016/j.jiec.2020.09.031**.

30 M. Romay, N. Diban, M. J. Rivero, A. Urtiaga and I. Ortiz, Critical Issues and Guidelines to Improve the Performance of Photocatalytic Polymeric Membranes, *Catalysts*, 2020, **10**(5), 570, DOI: **10.3390/catal10050570**.

31 A. Shokri and M. S. Fard, A Critical Review in Electrocoagulation Technology Applied for Oil Removal in Industrial Wastewater, *Chemosphere*, 2022, **288**, 132355, DOI: **10.1016/j.chemosphere.2021.132355**.

32 N. Hamzah and C. P. Leo, Fouling Prevention in the Membrane Distillation of Phenolic-Rich Solution Using Superhydrophobic PVDF Membrane Incorporated with TiO_2 Nanoparticles, *Sep. Purif. Technol.*, 2016, **167**, 79–87, DOI: **10.1016/j.seppur.2016.05.005**.

33 H. F. Tan, W. L. Tan, N. Hamzah, M. H. K. Ng, B. S. Ooi and C. P. Leo, Membrane Distillation Crystallization Using PVDF Membrane Incorporated with TiO_2 Nanoparticles and Nanocellulose, *Water Sci. Technol.: Water Supply*, 2020, **20**(5), 1629–1642, DOI: **10.2166/ws.2020.068**.

34 Y. K. Poon, S. K. Enche Ab Rahim, Q. H. Ng, P. Y. Hoo, N. Y. Abdullah, A. Nasib and N. S. Abdullah, Synthesis and Characterisation of Self-Cleaning TiO_2/PES Mixed Matrix Membranes in the Removal of Humic Acid, *Membranes*, 2023, **13**(4), 373, DOI: **10.3390/membranes13040373**.

35 ASTM E168-16. Standard practices for general techniques of infrared quantitative analysis, ASTM International, West Conshohocken, PA, USA, 2016.

36 ASTM E1252-98. Standard practice for general techniques for obtaining infrared spectra for qualitative analysis, ASTM International, West Conshohocken, PA, USA, 2021.

37 ASTM E3-11. Standard guide for preparation of metallographic specimens, ASTM International, ASTM International, West Conshohocken, PA, USA, 2017.

38 ASTM F3419-22. Standard test method for mineral characterization of equine surface materials by X-ray diffraction (XRD) techniques, ASTM International, West Conshohocken, PA, USA, 2022.

39 P. Boruah, R. Gupta and V. Katiyar, Fabrication of Cellulose Nanocrystal (CNC) from Waste Paper for Developing Antifouling and High-Performance Polyvinylidene Fluoride (PVDF) Membrane for Water Purification, *Carbohydr. Polym. Technol. Appl.*, 2023, **5**, 100309, DOI: **10.1016/j.carpta.2023.100309**.

40 A. Omar, I. Gomaa, O. A. Mohamed, H. Magdy, H. S. Kalloub, M. H. Hamza, T. M. Mohamed, M. M. Rabee, N. Tareq, H. Hesham, T. Abdallah, H. Elhaes and M. A. Ibrahim, Investigation of Morphological, Structural and Electronic Transformation of PVDF and ZnO/RGO/PVDF Hybrid Membranes, *Opt. Quantum Electron.*, 2023, **55**(4), 381, DOI: **10.1007/s11082-023-04663-6**.

41 ASTM E169-16. Standard practices for general techniques of ultraviolet-visible quantitative analysis, ASTM International, West Conshohocken, PA, USA, 2022.

42 L. Ruan, X. Yao, Y. Chang, L. Zhou, G. Qin and X. Zhang, Properties and Applications of the β Phase Poly(Vinylidene Fluoride), *Polymers*, 2018, **10**(3), 228, DOI: **10.3390/polym10030228**.

43 S. Kartohardjono, G. M. K. Salsabila, A. Ramadhani, I. Purnawan and W. J. Lau, Preparation of PVDF-PVP Composite Membranes for Oily Wastewater Treatment, *Membranes*, 2023, **13**(6), 611, DOI: **10.3390/membranes13060611**.

44 J. E. Marshall, A. Zhenova, S. Roberts, T. Petchey, P. Zhu, C. E. J. Dancer, C. R. McElroy, E. Kendrick and V. Goodship, On the Solubility and Stability of Polyvinylidene Fluoride, *Polymers*, 2021, **13**(9), 1354, DOI: **10.3390/polym13091354**.

45 T. Nishiyama, T. Sumihara, E. Sato and H. Horibe, Effect of Solvents on the Crystal Formation of Poly(Vinylidene Fluoride) Film Prepared by a Spin-Coating Process, *Polym. J.*, 2017, **49**(3), 319–325, DOI: **10.1038/pj.2016.116**.

46 F. Dai, Q. Zhuang, G. Huang, H. Deng and X. Zhang, Infrared Spectrum Characteristics and Quantification of OH Groups in Coal, *ACS Omega*, 2023, **8**(19), 17064–17076, DOI: **10.1021/acsomega.3c01336**.

47 Q. Cheng, A. Wang, Z. Song, J. Bao, J. Xue, Y. Wei, S. Li, L. Lv, J. Ding, M. Cai, J. Chen, Q. Wang, C. Gao and S. Sun, Enhancement and Stabilization of Isolated Hydroxyl Groups via the Construction of Coordinatively Unsaturated Sites on Surface and Subsurface of Hydrogenated TiO_2 Nanotube Arrays for Photocatalytic Complete Mineralization of Toluene, *J. Environ. Chem. Eng.*, 2021, **9**(2), 105080, DOI: **10.1016/j.jece.2021.105080**.

48 L. Y. Ng, T. J. Wong, C. Y. Ng and C. K. M. Amelia, A Review on Cellulose Nanocrystals Production and Characterization Methods from Elaeis Guineensis Empty Fruit Bunches, *Arabian J. Chem.*, 2021, **14**(9), 103339, DOI: **10.1016/j.arabjc.2021.103339**.

49 A. Mokhtari, M. Sabzi and H. Azimi, 3D Porous Bioadsorbents Based on Chitosan/Alginate/Cellulose Nanofibers as

Efficient and Recyclable Adsorbents of Anionic Dye, *Carbohydr. Polym.*, 2021, **265**, 118075, DOI: **10.1016/j.carbpol.2021.118075**.

50 S. Rashid and H. Dutta, Characterization of Nanocellulose Extracted from Short, Medium and Long Grain Rice Husks, *Ind. Crops Prod.*, 2020, **154**, 112627, DOI: **10.1016/j.indcrop.2020.112627**.

51 K. Nyamayaro, S. G. Hatzikiriakos and P. Mehrkhodavandi, Utilizing Cellulose-Based Conducting Hydrogels in Iontronics, *RSC Sustainability*, 2023, **1**(6), 1369–1385, DOI: **10.1039/d3su00139c**.

52 W. Rasri, V. T. Thu, A. Corpuz and L. T. Nguyen, Preparation and Characterization of Cellulose Nanocrystals from Corncob via Ionic Liquid [Bmim][HSO$_4$] Hydrolysis: Effects of Major Process Conditions on Dimensions of the Product, *RSC Adv.*, 2023, **13**(28), 19020–19029, DOI: **10.1039/D3RA02715E**.

53 X. Zhang, F. Li, X. Zhao, J. Cao, S. Liu, Y. Zhang, Z. Yuan, X. Huang, C. F. De Hoop, X. Peng and X. Huang, Bamboo Nanocellulose/Montmorillonite Nanosheets/Polyethyleneimine Gel Adsorbent for Methylene Blue and Cu(ii) Removal from Aqueous Solution, *Gels*, 2023, **9**(1), 40, DOI: **10.3390/gels9010040**.

54 C. D. Mino, A. J. Clancy, A. Sella, C. A. Howard, T. F. Headen, A. G. Seel and N. T. Skipper, Weak Interactions in Dimethyl Sulfoxide (DMSO)–Tertiary Amide Solutions: The Versatility of DMSO as a Solvent, *J. Phys. Chem. B*, 2023, **127**(6), 1357–1366, DOI: **10.1021/acs.jpcb.2c07155**.

55 D. Trache, A. F. Tarchoun, M. Derradji, T. S. Hamidon, N. Masruchin, N. Brosse and M. H. Hussin, Nanocellulose: From Fundamentals to Advanced Applications, *Front. Chem.*, 2020, **8**, 392, DOI: **10.3389/fchem.2020.00392**.

56 R. T. Varghese, R. M. Cherian, T. Antony, A. Tharayil, H. Das, H. Kargarzadeh, C. J. Chirayil and S. Thomas, A Review on the Best Bioadsorbent Membrane-Nanocellulose for Effective Removal of Pollutants from Aqueous Solutions, *Carbohydr. Polym. Technol. Appl.*, 2022, **3**, 100209, DOI: **10.1016/j.carpta.2022.100209**.

57 N. Nady, N. Salem and S. H. Kandil, Preparation and Characterization of a Novel Poly(Vinylidene Fluoride-Co-Hexafluoropropylene)/Poly(Ethersulfone) Blend Membrane Fabricated Using an Innovative Method of Mixing Electrospinning and Phase Inversion, *Polymers*, 2021, **13**(5), 790, DOI: **10.3390/polym13050790**.

58 A. Lopatina, M. Esmaeili, I. Anugwom, M. Mänttäri and M. Kallioinen-Mänttäri, Effect of Low Concentrations of Lithium Chloride Additive on Cellulose-Rich Ultrafiltration Membrane Performance, *Membranes*, 2023, **13**(2), 198, DOI: **10.3390/membranes13020198**.

59 S. Sakarkar, S. Muthukumaran and V. Jegatheesan, Tailoring the Effects of Titanium Dioxide (TiO$_2$) and Polyvinyl Alcohol (PVA) in the Separation and Antifouling Performance of Thin-Film Composite Polyvinylidene Fluoride (PVDF) Membrane, *Membranes*, 2021, **11**(4), 241, DOI: **10.3390/membranes11040241**.

60 X. Tan and D. Rodrigue, A Review on Porous Polymeric Membrane Preparation. Part1: Production Techniques with Polysulfone and Poly(Vinylidene Fluoride), *Polymers*, 2019, **11**(7), 1160, DOI: **10.3390/polym11071160**.

61 S. J. Bohr, F. Wang, M. Metze, J. L. Vukušić, A. Sapalidis, M. Ulbricht, B. Nestler and S. Barbe, State-of-the-Art Review of Porous Polymer Membrane Formation Characterization—How Numerical and Experimental Approaches Dovetail to Drive Innovation, *Front. Sustainability*, 2023, **4**, DOI: **10.3389/frsus.2023.1093911**.

62 A. I. Nazri, A. L. Ahmad and M. H. Hussin, Microcrystalline Cellulose-Blended Polyethersulfone Membranes for Enhanced Water Permeability and Humic Acid Removal, *Membranes*, 2021, **11**(9), 660, DOI: **10.3390/membranes11090660**.

63 F. Rafieian, M. Mousavi, A. Dufresne and Q. Yu, Polyethersulfone Membrane Embedded with Amine Functionalized Microcrystalline Cellulose, *Int. J. Biol. Macromol.*, 2020, **164**, 4444–4454, DOI: **10.1016/j.ijbiomac.2020.09.017**.

64 Z. Wu, X. Ji, Q. He, H. Gu, W. Zhang and Z. Deng, Nanocelluloses Fine-Tuned Polyvinylidene Fluoride (PVDF) Membrane for Enhanced Separation and Antifouling, *Carbohydr. Polym.*, 2024, **323**, 121383, DOI: **10.1016/j.carbpol.2023.121383**.

65 N. B. Darwish, A. Alkhudhiri, H. AlRomaih, A. Alalawi, M. C. Leaper and N. Hilal, Effect of Lithium Chloride Additive on Forward Osmosis Membranes Performance, *J. Water Process Eng.*, 2020, **33**, 101049, DOI: **10.1016/j.jwpe.2019.101049**.

66 Z. Li, P. Zhang, K. Guan, T. Yoshioka and H. Matsuyama, Water Flux Enhancement of PVDF Membrane by a Facile Coating Method for Vacuum Membrane Distillation, *Desalination*, 2022, **536**, 115818, DOI: **10.1016/j.desal.2022.115818**.

67 M. Yang, P. Hadi, X. Yin, J. Yu, X. Huang, H. Ma, H. Walker and B. S. Hsiao, Antifouling Nanocellulose Membranes: How Subtle Adjustment of Surface Charge Lead to Self-Cleaning Property, *J. Membr. Sci.*, 2021, **618**, 118739, DOI: **10.1016/j.memsci.2020.118739**.

68 A. Morsy, A. S. Mahmoud, A. Soliman, H. Ibrahim and E. Fadl, Improved Anti-Biofouling Resistances Using Novel Nanocelluloses/Cellulose Acetate Extracted from Rice Straw Based Membranes for Water Desalination, *Sci. Rep.*, 2022, **12**(1), 4386, DOI: **10.1038/s41598-022-08324-8**.

69 P. Hadi, M. Yang, H. Ma, X. Huang, H. Walker and B. S. Hsiao, Biofouling-Resistant Nanocellulose Layer in Hierarchical Polymeric Membranes: Synthesis, Characterization and Performance, *J. Membr. Sci.*, 2019, **579**, 162–171, DOI: **10.1016/j.memsci.2019.02.059**.

70 S. S. Jaffar, S. Saallah, M. Misson, S. Siddiquee, J. Roslan, S. Saalah and W. Lenggoro, Recent Development and Environmental Applications of Nanocellulose-Based Membranes, *Membranes*, 2022, **12**(3), 287, DOI: **10.3390/membranes12030287**.

71 J. Wang, H. Song, L. Ren, M. E. Talukder, S. Chen and J. Shao, Study on the Preparation of Cellulose Acetate Separation Membrane and New Adjusting Method of Pore Size, *Membranes*, 2021, **12**(1), 9, DOI: **10.3390/membranes12010009**.

72 A. A. James, M. R. Rahman, D. Huda, M. M. Rahman, J. Uddin, M. K. B. Bakri and A. Chanda, Optimization of Novel Nanocomposite Powder for Simultaneous Removal of Heavy Metals from Palm Oil Mill Effluent (POME) by Response Surface Methodology (RSM), *Environ. Dev. Sustain.*, 2023, **26**(2), 3589–3615, DOI: **10.1007/s10668-022-02849-8**.

73 M. Batool, A. Shafeeq, B. Haider and N. M. Ahmad, TiO_2 Nanoparticle Filler-Based Mixed-Matrix PES/CA Nanofiltration Membranes for Enhanced Desalination, *Membranes*, 2021, **11**(6), 433, DOI: **10.3390/membranes11060433**.

74 N. H. Khdary, B. T. Almuarqab and G. El Enany, Nanoparticle-Embedded Polymers and Their Applications: A Review, *Membranes*, 2023, **13**(5), 537, DOI: **10.3390/membranes13050537**.

75 Z. M. H. M. Shafie, A. L. Ahmad, S. C. Low, S. Rode and B. Belaissaoui, Lithium Chloride (LiCl)-Modified Polyethersulfone (PES) Substrate Surface Pore Architectures on Thin Poly(Dimethylsiloxane) (PDMS) Dense Layer Formation and the Composite Membrane's Performance in Gas Separation, *RSC Adv.*, 2020, **10**(16), 9500–9511, DOI: **10.1039/D0RA00045K**.

76 D.-T. Tran, J.-P. Méricq, J. Mendret, S. Brosillon and C. Faur, Influence of Preparation Temperature on the Properties and Performance of Composite $PVDF-TiO_2$ Membrane, *Membranes*, 2021, **11**(11), 876, DOI: **10.3390/membranes11110876**.

77 N. Hamzah and C. P. Leo, Membrane Distillation of Saline with Phenolic Compound Using Superhydrophobic PVDF Membrane Incorporated with TiO_2 Nanoparticles: Separation, Fouling and Self-Cleaning Evaluation, *Desalination*, 2017, **418**, 79–88, DOI: **10.1016/j.desal.2017.05.029**.

78 D. Matveev, I. Borisov, V. Vasilevsky, G. Karpacheva and V. Volkov, Spinning of Polysulfone Hollow Fiber Membranes Using Constant Dope Solution Composition: Viscosity Control via Temperature, *Membranes*, 2022, **12**(12), 1257, DOI: **10.3390/membranes12121257**.

79 L. Solhi, V. Guccini, K. Heise, I. Solala, E. Niinivaara, W. Xu, K. Mihhels, M. Kröger, Z. Meng, J. Wohlert, H. Tao, E. D. Cranston and E. Kontturi, Understanding Nanocellulose-Water Interactions: Turning a Detriment into an Asset, *Chem. Rev.*, 2023, **123**(5), 1925–2015, DOI: **10.1021/acs.chemrev.2c00611**.

80 M. I. Baig, J. D. Willott and W. M. de Vos, Tuning the Structure and Performance of Polyelectrolyte Complexation Based Aqueous Phase Separation Membranes, *J. Membr. Sci.*, 2020, **615**, 118502, DOI: **10.1016/j.memsci.2020.118502**.

81 R. Rohani, I. I. Yusoff and V. Manimaran, Polyvinylidene Difluoride-*Co*-Polyethylene Glycol Membrane for Biohydrogen Purification from Palm Oil Mill Effluent Fermentati, *J. Membr. Sci. Res.*, 2021, 166–172.

82 X. Zi, H. Wu, J. Song, W. He, L. Xia, J. Guo, S. Luo and W. Yan, Electrospun Sandwich-like Structure of PVDF-HFP/Cellulose/PVDF-HFP Membrane for Lithium-Ion Batteries, *Molecules*, 2023, **28**(13), 4998, DOI: **10.3390/molecules28134998**.

83 Z. Arif, N. K. Sethy, L. Kumari, P. K. Mishra and B. Verma, Antifouling Behaviour of $PVDF/TiO_2$ Composite Membrane: A Quantitative and Qualitative Assessment, *Iran. Polym. J.*, 2019, **28**(4), 301–312, DOI: **10.1007/s13726-019-00700-y**.

84 S. Mohammadpourfazeli, S. Arash, A. Ansari, S. Yang, K. Mallick and R. Bagherzadeh, Future Prospects and Recent Developments of Polyvinylidene Fluoride (PVDF) Piezoelectric Polymer; Fabrication Methods, Structure, and Electro-Mechanical Properties, *RSC Adv.*, 2023, **13**(1), 370–387, DOI: **10.1039/D2RA06774A**.

85 K.-Y. Chan, C.-L. Li, D.-M. Wang and J.-Y. Lai, Formation of Porous Structures and Crystalline Phases in Poly-(Vinylidene Fluoride) Membranes Prepared with Nonsolvent-Induced Phase Separation-Roles of Solvent Polarity, *Polymers*, 2023, **15**(5), 1314, DOI: **10.3390/polym15051314**.

86 Y. Zhou, W. Liu, B. Tan, C. Zhu, Y. Ni, L. Fang, C. Lu and Z. Xu, Crystallinity and β Phase Fraction of PVDF in Biaxially Stretched PVDF/PMMA Films, *Polymers*, 2021, **13**(7), 998, DOI: **10.3390/polym13070998**.

87 S. L. Moffitt, P. Pan, L. Perry, J. Tracy, K. R. Choudhury, M. D. Kempe and X. Gu, Microstructure Changes during Failure of PVDF-based Photovoltaic Backsheets, *Prog. Photovoltaics Res. Appl.*, 2023, **31**(1), 26–35, DOI: **10.1002/pip.3605**.

88 S. Uličná, M. Owen-Bellini, S. L. Moffitt, A. Sinha, J. Tracy, K. Roy-Choudhury, D. C. Miller, P. Hacke and L. T. Schelhas, A Study of Degradation Mechanisms in PVDF-Based Photovoltaic Backsheets, *Sci. Rep.*, 2022, **12**(1), 14399, DOI: **10.1038/s41598-022-18477-1**.

89 J. Lv, G. Zhang, H. Zhang, C. Zhao and F. Yang, Improvement of Antifouling Performances for Modified PVDF Ultrafiltration Membrane with Hydrophilic Cellulose Nanocrystal, *Appl. Surf. Sci.*, 2018, **440**, 1091–1100, DOI: **10.1016/j.apsusc.2018.01.256**.

90 W. Zhang, G. Wu, H. Zeng, Z. Li, W. Wu, H. Jiang, W. Zhang, R. Wu, Y. Huang and Z. Lei, The Preparation, Structural Design, and Application of Electroactive Poly(Vinylidene Fluoride)-Based Materials for Wearable Sensors and Human Energy Harvesters, *Polymers*, 2023, **15**(13), 2766, DOI: **10.3390/polym15132766**.

91 A. Etale, A. J. Onyianta, S. R. Turner and S. J. Eichhorn, Cellulose: A Review of Water Interaction, Applications in Composites, and Water Treatment, *Chem. Rev.*, 2023, **123**(5), 2016–2048, DOI: **10.1021/acs.chemrev.2c00477**.

92 A. Kamtsikakis, G. Delepierre and C. Weder, Cellulose Nanocrystals as a Tunable Nanomaterial for Pervaporation Membranes with Asymmetric Transport Properties, *J. Membr. Sci.*, 2021, **635**, 119473, DOI: **10.1016/j.memsci.2021.119473**.

93 R. Ahmad, C. S. Lee, J. H. Kim and J. Kim, Partially Coated TiO_2 on Al_2O_3 Membrane for High Water Flux and Photodegradation by Novel Filtration Strategy in Photocatalytic Membrane Reactors, *Chem. Eng. Res. Des.*, 2020, **163**, 138–148, DOI: **10.1016/j.cherd.2020.08.027**.

94 M. J. Azad, A. R. Pouranfard, D. Emadzadeh, W. J. Lau and E. Alipanahpour Dil, Simulation of Forward Osmosis and Pressure Retarded Osmosis Membrane Performance: Effect of TiO_2 Nanoparticles Loading on the Semi-Permeable

Membrane, *Comput. Chem. Eng.*, 2022, **160**, 107709, DOI: **10.1016/j.compchemeng.2022.107709**.

95 J. Liang, K. Gao, A. Zhou, Y. Fang, S. Su, L. Fu, M. Sun and X. Duan, Long-Lasting Performance of High-Flux Perovskite Membrane for Catalytic Degradation of Organic Pollutants, *Appl. Catal., B*, 2023, **327**, 122440, DOI: **10.1016/j.apcatb.2023.122440**.

96 C. Lin, L. Chung, G. Lin, M.-C. Chang, C.-Y. Lee and N.-H. Tai, Enhancing the Efficiency of a Forward Osmosis Membrane with a Polydopamine/Graphene Oxide Layer Prepared via the Modified Molecular Layer-by-Layer Method, *ACS Omega*, 2020, **5**(30), 18738–18745, DOI: **10.1021/acsomega.0c01752**.

97 R. Abedini, S. M. Mousavi and R. Aminzadeh, A Novel Cellulose Acetate (CA) Membrane Using TiO$_2$ Nanoparticles: Preparation, Characterization and Permeation Study, *Desalination*, 2011, **277**(1–3), 40–45, DOI: **10.1016/j.desal.2011.03.089**.

98 N. Mahdhi, N. S. Alsaiari, A. Amari and M. A. Chakhoum, Effect of TiO$_2$ Nanoparticles on Capillary-Driven Flow in Water Nanofilters Based on Chitosan Cellulose and Polyvinylidene Fluoride Nanocomposites: A Theoretical Study, *Polymers*, 2022, **14**(14), 2908, DOI: **10.3390/polym14142908**.

99 A. Haleem, A. Shafiq, S.-Q. Chen and M. Nazar, A Comprehensive Review on Adsorption, Photocatalytic and Chemical Degradation of Dyes and Nitro-Compounds over Different Kinds of Porous and Composite Materials, *Molecules*, 2023, **28**(3), 1081, DOI: **10.3390/molecules28031081**.

100 J. Cheng, C. Zhan, J. Wu, Z. Cui, J. Si, Q. Wang, X. Peng and L.-S. Turng, Highly Efficient Removal of Methylene Blue Dye from an Aqueous Solution Using Cellulose Acetate Nanofibrous Membranes Modified by Polydopamine, *ACS Omega*, 2020, **5**(10), 5389–5400, DOI: **10.1021/acsomega.9b04425**.

101 X. Du, Y. Shi, V. Jegatheesan and I. U. Haq, A Review on the Mechanism, Impacts and Control Methods of Membrane Fouling in MBR System, *Membranes*, 2020, **10**(2), 24, DOI: **10.3390/membranes10020024**.

102 R. Zylla, M. Foszpańczyk, I. Kamińska, M. Kudzin, J. Balcerzak and S. Ledakowicz, Impact of Polymer Membrane Properties on the Removal of Pharmaceuticals, *Membranes*, 2022, **12**(2), 150, DOI: **10.3390/membranes12020150**.

103 Y. Zhang, H. Zhang, S. Tian, L. Zhang, W. Li, W. Wang, X. Yan, N. Han and X. Zhang, The Photocatalysis-Enhanced TiO$_2$@HPAN Membrane with High TiO$_2$ Surface Content for Highly Effective Removal of Cationic Dyes, *Langmuir*, 2021, **37**(31), 9415–9428, DOI: **10.1021/acs.langmuir.1c01066**.

104 A. A. James, M. R. Rahman, D. Huda, F. M. Aqlan, M. M. Matin, M. K. B. Bakri, K. K. Kuok and M. M. Rahman, Synthesis and Characterization of Novel Nano-Carbon Mixture from Dabai (Canarium Odontophyllum) Nutshell, *BioResources*, 2022, **17**(3), 4452–4469, DOI: **10.15376/biores.17.3.4452-4469**.

105 Md. R. Rahman, A. A. James, A.-K. Othman, M. K. bin; Bin Bakri, J. Uddin, A. Z. Sueraya, M. M. Matin, S. Y. Alfaifi, O. Madkhali, M. D. Aljabri and M. M. Rahman, Extraction and Characterization of Modified Algae Derivative Cellulose and Its Mixtures for Dye Removal, *BioResources*, 2023, **18**(3), 5967–5992, DOI: **10.15376/biores.18.3.5967-5992**.

106 N. H. Othman, N. H. Alias, M. Z. Shahruddin, N. F. Abu Bakar, N. R. Nik Him and W. J. Lau, Adsorption Kinetics of Methylene Blue Dyes onto Magnetic Graphene Oxide, *J. Environ. Chem. Eng.*, 2018, **6**(2), 2803–2811, DOI: **10.1016/j.jece.2018.04.024**.

107 U. Fathanah, S. Muchtar, S. Aprilia, M. R. Lubis, S. Mulyati and M. Yusuf, Unlocking Synergies of Mg(OH)$_2$ and Rice Husk Silica as Dual Additives for Tailored Pore Properties, Selectivity, and Antifouling Performances of PES Membrane, *S. Afr. J. Chem. Eng.*, 2024, **48**, 22–29, DOI: **10.1016/j.sajce.2024.01.004**.

108 P. García-Ramírez and L. A. Diaz-Torres, Self-Cleaning Cellulose Acetate/Crystalline Nanocellulose/Polyvinylidene Fluoride/Mg0.975Ni0.025SiO3 Membrane for Removal of Diclofenac Sodium and Methylene Blue Dye in Water, *Nanotechnology*, 2024, **35**(1), 015703, DOI: **10.1088/1361-6528/acfd32**.

109 A. M. Nasir, M. R. Adam, S. N. E. A. Mohamad Kamal, J. Jaafar, M. H. D. Othman, A. F. Ismail, F. Aziz, N. Yusof, M. R. Bilad, R. Mohamud, M. A. Rahman and W. N. Wan Salleh, A Review of the Potential of Conventional and Advanced Membrane Technology in the Removal of Pathogens from Wastewater, *Sep. Purif. Technol.*, 2022, **286**, 120454, DOI: **10.1016/j.seppur.2022.120454**.

110 V. O. Mkpuma, N. R. Moheimani, K. Fischer, A. Schulze and H. Ennaceri, Membrane Surface Zwitterionization for an Efficient Microalgal Harvesting: A Review, *Algal Res.*, 2022, **66**, 102797, DOI: **10.1016/j.algal.2022.102797**.

111 S. Tabraiz, M. Zeeshan, M. B. Asif, U. Egwu, S. Iftekhar and P. Sallis, Membrane Bioreactor for Wastewater Treatment: Fouling and Abatement Strategies, *Current Developments in Biotechnology and Bioengineering*, Elsevier, 2023, pp. 173–202, DOI: **10.1016/B978-0-443-19180-0.00012-2**.

112 N. G. Cogan, D. Ozturk, K. Ishida, J. Safarik and S. Chellam, Membrane Aging Effects on Water Recovery during Full-Scale Potable Reuse: Mathematical Optimization of Backwashing Frequency for Constant-Flux Microfiltration, *Sep. Purif. Technol.*, 2022, **286**, 120294, DOI: **10.1016/j.seppur.2021.120294**.

113 E. Y. C. Yan, S. Zakaria, C. H. Chia and T. Rosenau, Bifunctional Regenerated Cellulose Membrane Containing TiO$_2$ Nanoparticles for Absorption and Photocatalytic Decomposition, *Sains Malaysiana*, 2017, **4**, 637–644, DOI: **10.17576/jsm-2017-4604-017**.

114 M. Homocianu and P. Pascariu, High-Performance Photocatalytic Membranes for Water Purification in Relation to Environmental and Operational Parameters, *J. Environ. Manage.*, 2022, **311**, 114817, DOI: **10.1016/j.jenvman.2022.114817**.

115 M. H. Abdellah, S. A. Nosier, A. H. El-Shazly and A. A. Mubarak, Photocatalytic Decolorization of Methylene Blue Using TiO$_2$/UV System Enhanced by Air Sparging, *Alexandria Eng. J.*, 2018, **57**(4), 3727–3735, DOI: **10.1016/j.aej.2018.07.018**.

116 M. S. Cergel, E. Demir and F. Atay, The Effect of the Structural, Optical, and Surface Properties of Anatase-TiO$_2$ Film on Photocatalytic Degradation of Methylene Blue Organic Contaminant, *Ionics*, 2019, **25**(9), 4481–4492, DOI: **10.1007/s11581-019-02986-7**.

117 M. Pavel, C. Anastasescu, R.-N. State, A. Vasile, F. Papa and I. Balint, Photocatalytic Degradation of Organic and Inorganic Pollutants to Harmless End Products: Assessment of Practical Application Potential for Water and Air Cleaning, *Catalysts*, 2023, **13**(2), 380, DOI: **10.3390/catal13020380**.

118 Z. Li and P. Yang, Review on Physicochemical, Chemical, and Biological Processes for Pharmaceutical Wastewater, *IOP Conf. Ser. Earth Environ. Sci.*, 2018, **113**, 012185, DOI: **10.1088/1755-1315/113/1/012185**.

119 N. F. Ishak, N. A. Hashim and M. H. D. Othman, Antifouling Properties of Hollow Fibre Alumina Membrane Incorporated with Graphene Oxide Frameworks, *J. Environ. Chem. Eng.*, 2020, **8**(4), 104059, DOI: **10.1016/j.jece.2020.104059**.

120 Z. Wang, G. Feng, Z. Yan, S. Li, M. Xu, C. Wang and Y. Li, Improving the Hydrophilicity and Antifouling Performance of PVDF Membranes via PEI Amination and Further Poly(Methyl Vinyl Ether-Alt-Maleic Anhydride) Modification, *React. Funct. Polym.*, 2023, **189**, 105610, DOI: **10.1016/j.reactfunctpolym.2023.105610**.

121 M. G. Nainar, K. Jayaraman, H. K. Meyyappan and L. R. Miranda, Antifouling Properties of Poly(Vinylidene Fluoride)-Incorporated Cellulose Acetate Composite Ultrafiltration Membranes, *Korean J. Chem. Eng.*, 2020, **37**(12), 2248–2261, DOI: **10.1007/s11814-020-0653-8**.

122 E. Pramono, K. Umam, F. Sagita, O. A. Saputra, R. Alfiansyah, R. S. Setyawati Dewi, G. T. M. Kadja, M. Ledyastuti, D. Wahyuningrum and C. L. Radiman, The Enhancement of Dye Filtration Performance and Antifouling Properties in Amino-Functionalized Bentonite/Polyvinylidene Fluoride Mixed Matrix Membranes, *Heliyon*, 2023, **9**(1), e12823, DOI: **10.1016/j.heliyon.2023.e12823**.